UC San Diego

UC San Diego Electronic Theses and Dissertations

Title

Passivation of Interface Defects on GaAs and InGaAs (001) and (110) Surfaces and Improvement of Low Temperature HfO_2 ALD Nucleation

Permalink

https://escholarship.org/uc/item/41b162wk

Author

Kent, Tyler James

Publication Date

2015

Peer reviewed|Thesis/dissertation

eScholarship.org Powered by the California Digital Library
University of California

UNIVERSITY OF CALIFORNIA, SAN DIEGO

Passivation of Interface Defects on GaAs and InGaAs (001) and (110) Surfaces and Improvement of Low Temperature HfO_2 ALD Nucleation

A dissertation submitted in partial satisfaction of the requirements for the degree
Doctor of Philosophy

in

Materials Science and Engineering

by

Tyler James Kent

Committee in Charge:

Professor Andrew C. Kummel, Chair
Professor Peter M. Asbeck
Professor Vitali F. Nesterenko
Professor William C. Trogler
Professor Paul K. Yu

2015

Copyright ©

Tyler James Kent, 2015

All Rights Reserved

The Dissertation of Tyler James Kent is approved, and it is acceptable in quality and form for publication on microfilm and electronically:

____

____

____

____

____
Chair

University of California, San Diego

2015

DEDICATION

To my Mom and Dad, whose guidance, love, and support have encouraged me and allowed me to push myself in all aspects of life.

EPIGRAPH

Energy and persistence conquer all things.

Benjamin Franklin

TABLE OF CONTENTS

Signature Page....................iii

Dedication....................iv

Epigraph....................v

Table of Contents....................vi

List of Symbols and Abbreviations....................ix

List of Figures....................xii

List of Tables....................xv

Acknowledgments....................xvi

Vita. xix

Abstract of the Dissertation....................xxii

Chapter 1....................1
Introduction

1.1 Trap states at the semiconductor/oxide interface....................1

1.2 Ultra high vacuum chamber....................2

1.3 Scanning tunneling microscopy....................3

1.4 Scanning tunneling spectroscopy....................4

1.5 X-ray photoelectron spectroscopy....................5

1.6 Capacitance voltage measurements....................6

1.7 Density functional theory....................7

1.8 References....................11

Chapter 2..12
Dual Passivation of Intrinsic Defects at the Compound Semiconductor/Oxide Interface Using an Oxidant and a Reductant

2.1 Abstract..12

2.2 Introduction...13

2.3 Methods...15

2.4 Results and Discussion..16

2.4.1 DFT simulations 16

2.4.2 STM/STS...18

2.5 Conclusions..21

2.6 Acknowledgements..22

2.7 Supplemental material...22

2.8 References..40

Chapter 3..42
Dual passivation of GaAs (110) surfaces using O_2/H_2O and trimethylaluminum

3.1 Abstract..42

3.2 Introduction...43

3.3 Experimental..45

3.4 Results and discussion...47

3.4.1 STM of TMA deposition on GaAs (110) surface...................................47

3.4.2 STS of TMA deposition on GaAs (110) surface....................................52

3.4.3 DFT simulations...54

3.5 Conclusion...56

3.6 Acknowledgments..57

3.7 References..71

Chapter 4...**73**
The Influence of wet and dry native oxide removal on the nucleation of low temperature HfO_2 ALD on InGaAs (001) and (110) surfaces

4.1 Abstract...73

4.2 Introduction..74

4.3 Experimental...76

4.4 Results and Discussion...78

4.4.1 *In situ* native oxide/contaminant removal...78

4.4.2 *Ex situ* native oxide removal..82

4.5 Conclusion..87

4.6 Acknowledgements..87

4.7 References...97

LIST OF SYMBOLS AND ABBREVIATIONS

Å	angstrom
AFM	atomic force microscopy
ALD	atomic layer deposition
BE	binding energy
BOE	buffered oxide etch
CB	conduction band
CG	conjugate gradient
C_{max}	maximum capacitance
CV	capacitance voltage
CVD	chemical vapor deposition
DFT	density functional theory
DI	deionized
D_{it}	density of interface traps
DMA	dimethylaluminum
DOS	density of states
e	electron
E_f	Fermi level
EOT	equivalent oxide thickness
FGA	forming gas anneal
GV	conductance voltage
h	Planck's constant

I	electric current
IPA	isopropylalcohol
KE	kinetic energy
L	Langmuir
LDOS	local density of states
LEED	low energy electron diffraction
MBE	molecular beam epitaxy
MMA	monomethylaluminum
MOSCAP	metal oxide semiconductor capacitor
MOSFET	metal oxide semiconductor field effect transistor
N_{bt}	border trap density
nm	nanometer
pA	picoamps
PAW	projector augmented wave
PBE	Perdew-Burke-Emzerhof
PBN	pyrolitic boron nitride
PDA	post deposition anneal
PP	pseudo potential
SPM	scanning probe microscopy
SRC	Semiconductor Research Corporation
STM	scanning tunneling microscopy
TEMAH	tetrakis(ethylmethylamino)hafnium

TMA	trimethylaluminum
TMG	trimethylgallium
UHV	ultra high vacuum
V	volts
VASP	Vienna ab-initio simulation package
VB	valence band
V_{fb}	flatband voltage
V_{th}	threshold voltage
XPS	x-ray photoelectron spectroscopy
υ	frequency
Φ_{spec}	spectrometer work function

LIST OF FIGURES

Figure 1.2. Schematic diagram of Omicron Variable temperature UHV chamber.........8

Figure 1.3. Schematic representations and band diagrams of filled and empty state STM imaging...9

Figure 1.6. Schematic diagram of MOSCAP...10

Figure 2.1. Side view of relaxed DFT model of TMA passivated InGaAs (2x4) α2 unit cell and DOS...26

Figure 2.2. Side view of relaxed DFT models and DOS of –O, -S, -NH passivated InGaAs (2x4) α2 unit cell..27

Figure 2.3. Side view of relaxed DFT models and DOS of double –OH, -SH, $-NH_2$ passivated InGaAs (2x4) α2 unit cell..28

Figure 2.4. Side view of relaxed DFT models and DOS of quadruple –OH, -SH, $-NH_2$ passivated InGaAs (2x4) α2 unit cell..29

Figure 2.5. Filled state STM images of clean and –OH passivated (2x4) surface...30

Figure 2.6. 100 x 100 nm^2 filled state STM image of HOOH and TMA passivated InGaAs (2x4) surface...31

Figure 2.7. STS spectra of clean (2x4) surface and TMA/HOOH passivated surface...32

Figure 2.8. STS curves of n and p-type HOOH and TMA passivated InGaAs (2x4) surface..33

Figure 2.9. 20 x 100 nm^2 filled state STM image and STS curves TMA + H_2O dosed surface..34
Figure 2.10. STS curves of n and p-type samples initially dosed with TMA and then H_2O..35
Figure 2.11. DFT model of InGaAs bulk super cell and calculated DOS...................36
Figure 2.12. DFT model and calculated DOS for clean missing dimer unit cell and DMA passivated unit cell with random In/Ga distribution.....................37
Figure 2.13. DFT simulations of two O/S atoms inserted into the metallic bond and two and -OH/-SH on the edge In/Ga..38
Figure 2.14. DFT model of quadruple –OH, -SH, and –NH_2 passivated α2 unit cell with In surface segregation...39
Figure 3.1. Filled state STM image and ball and stick model of clean GaAs (110) surface..58
Figure 3.2. STM image of low coverage TMA / GaAs (110) surface.........................59
Figure 3.3. STM of 10 L dose of TMA on GaAs (110)...60
Figure 3.4. STM image of complete TMA monolayer on GaAs (110).......................61
Figure 3.5. STM images of annealing study after 500 L TMA deposition..................62
Figure 3.6. Filled state STM image of DMA/GaAs (110) surfaces dosed with O_2......63
Figure 3.7. STS spectra of clean and full coverage TMA surface...............................64
Figure 3.8. STS comparison of full coverage TMA and O_2/H_2O passivated surface...65
Figure 3.9. STS spectra of clean InGaAs (110) surface after Al_2O_3 deposition...........66

Figure 3.10. DFT model and calculated DOS for clean GaAs (110) TMA passivated GaAs (110), and O/-OH passivated GaAs (110).....................................67

Figure 3.11. Side views of DFT model of defect site on TMA passivated GaAs (110)..68

Figure 3.12. Ball and stick model of improper DMA chemisorption on GaAs (110)..69

Figure 3.13. XPS peaks and corrected areas for Al 2s and O 1s after TMA deposition..70

Figure 4.1. CV curves obtained after H and H/TMA/H pre-ALD surface clean..........88

Figure 4.2. STM images of InGaAs (2x4) surface before, during, and after H/TMA/H surface clean..89

Figure 4.3. CV curves obtained after the number of pre-ALD H/TMA/H cycles were varied..90

Figure 4.4. CV curves of InGaAs (001) samples which did and did not receive BOE immediately prior to ALD at 120 ˚C..91

Figure 4.5. CV curves of InGaAs (001) samples which did and did not receive BOE immediately prior to ALD at 300 ˚C..92

Figure 4.6. leakage current density curves of wet and non-wet cleaned (001) and (110) samples at 120 ˚C and 300 ˚C..93

Figure 4.7. XPS data before, during, and after H/TMA/H pre-ALD surface clean..94

Figure 4.8. D_{it} extracted using the full interface state model.......................................95

LIST OF TABLES

Table 4.1. V_{fb}, C_{ox}, N_{bt}, and D_{it} data for all samples in chapter 4................................96

ACKNOWLEDGEMENTS

I would like to acknowledge my advisor, Professor Andy Kummel, who has allowed the graduate school experience to be an extremely enjoyable and enlightening one. Being able to attend a large number of conferences and have access to quality equipment in the lab made all collaborations and most of the experimentation fun.

I would also like to acknowledge former members of the Kummel group, namely, Dr. Wil Melitz who took me under his wing. It was extremely motivating to work with someone as intelligent as Wil and I attribute a lot of my abilities to his teaching skills. Dr. Tobin Kaufman-Osborn was also a great friend who helped me find solutions to difficult problems in lab. Outside of lab he was my partner in crime and there are a plethora of memories that will not be forgotten. I also want to thank Dr. Jim Royer for allowing me to talk about surfing with someone other than myself, it was awesome being able to walk out of lab and be surfing Blacks in 5 minutes with him. Finally, Dr. Alex Liberman who was always willing to have a beverage after a long weeks work. Tobin, Wil, Jim, and Alex made living in San Diego a joy and I will never forget the good times had with them. Mary Edmonds was a great teammate and I enjoyed, as much as one can with vacuum equipment, working with her on our chamber. I also would like to thank the other Kummel group members who I have enjoyed spending time with in and out of lab; Jun Hong Park, Dr. Evgeniy Chagarov, Sang Wook Park, Natalie Mendez, Il Jo Qwak, Kasra Sardashti, Katty Hu, Steve Wolf, and Hyunwoong Kim.

I would not be writing this dissertation if it had not been for the help of our many collaborators. Professor Ravi Droopad deserves an enormous thanks for growing us endless supplies of high quality MBE InGaAs. Cheng-Ying Huang, Dr. Sanghoon Lee, Varisthna (Gift) Chobpattana, and Professor Mark Rodwell helped me to gain an understanding of device fabrication and electrical characterization. Dr. Jaesoo Ahn, Kechao Tang, Adi Negara, and Professor Paul McIntyre deserve thanks for their help in measuring and analyzing numerous CV curves as well as many useful discussions.

My committee deserves huge thanks for giving up their precious time to attend my Senate and Thesis Defense presentations. The committee includes Professor Paul Yu, Professor William Trogler, Professor Vitali Nesternenko, and Professor Peter Asbeck.

I would like to thank my family; Rob, Anne, Ryan, and Victoria Kent for their support throughout these five years and my whole life. My girlfriend, Andrea Zamucen, deserves tremendous thanks for always cheering me up after a hard day. And my roommates for always providing an entertaining atmosphere to come home to.

This work was funded by the Semiconductor Research Corporation and from custom funding projects from many of the constituent member companies including Applied Materials and Global Foundries.

Chapter 2, in part or in full, is a reprint of the following material:

T. Kent, M. Edmonds, E. Chagarov, R. Droopad, A. C. Kummel "Dual passivation of intrinsic defects at the compound semiconductor/oxide interface using an oxidant and

a reductant" ACS nano *(In Press)* 2015. The dissertation author was the primary investigator and author of this paper.

Chapter 3, in part or in full, is a reprint of the material as it appears in The Journal of Chemical Physics. T. Kent, M. Edmonds, E. Chagarov, R. Droopad, A. C. Kummel "Dual passivation of GaAs (110) surfaces using O_2/H_2O and trimethylaluminum." (2013) The Journal of Chemical Physics **139**(24): 244706. The dissertation author was the primary investigator and author of this paper.

Chapter 4 is in part or full, reprinted with permission from T. Kent, K. Tang, V. Chobpattana, M. A. Negara, M. Edmonds, B. Sahu, R. Galatage, W. Mitchell, R. Droopad, P. McIntyre, and A. C. Kummel, "The Influence of wet and dry native oxide removal on the nucleation of low temperature HfO_2 ALD on InGaAs (001) and (110) surfaces". Manuscript in preparation. The dissertation/thesis author was the primary investigator and author of this paper.

VITA

EDUCATION

2010 Bachelor of Science in Chemistry, University of California, Santa Barbara

2011 Master of Science in Materials Science and Engineering, University of California, San Diego

2015 Doctor of Philosophy in Materials Science and Engineering, University of California, San Diego

PUBLICATIONS

T. Kent, M. Edmonds, et al. (2014). "InGaAs (110) surface cleaning using atomic hydrogen". Solid State Phenomena, Trans Tech Publ.

T. Kent, K. Tang, M.A. Negara, V. Chobpattana, P. McIntyre, R. Droopad, A. C. Kummel "The effects of InGaAs native oxide removal techniques on the nucleation of low temperature HfO_2 ALD", *(manuscript in preparation)*

T. Kent, M. Edmonds, E. Chagarov, R. Droopad, A. C. Kummel "Dual passivation of intrinsic defects at the compound semiconductor/oxide interface using an oxidant and a reductant" ACS nano *(In Press)* 2015

T. Kent, M. Edmonds, E. Chagarov, R. Droopad, A. C. Kummel "Dual passivation of GaAs (110) surfaces using O_2/H_2O and trimethylaluminum." (2013 The Journal of Chemical Physics 139(24): 244706.

T. Kent, K. Tang, M. A. Negara, C. Y. Huang, S. Lee, V. Chobpattana, P. McIntyre, R. Droopad, A. C. Kummel "The effects of InGaAs (110) and (001) surface cleans on the nucleation of low temperature HfO_2 ALD" Techcon 2014 Austin, TX

T. Kent, M. Edmonds, E. Chagarov, and A. C. Kummel. "Dual Passivation of the GaAs (110) Surface using TMA/O_2" Techcon 2013 Austin, TX P066925

Ahn, J., T. Kent, et al. (2013). "Arsenic decapping and pre-atomic layer deposition trimethylaluminum passivation of Al_2O_3/InGaAs (100) interfaces." Applied Physics Letters 103(7): 071602.

“Surface Preparation and In/Ga Alloying Effects on InGaAs (001)-(2x4) Surfaces for ALD Gate Oxide Deposition” M. Edmonds, T. Kent, E. Chagarov, A.C. Kummel. ECS Transactions 50 (4) 129-140 (2012).

“Atomic imaging of atomic layer deposition oxide nucleation with trimethylaluminum on As-rich InGaAs(001) 2×4 vs. Ga/In-rich InGaAs(001) 4×2” W. Melitz, T. Kent, A. C. Kummel, R. Droopad, M. Holland, I. Thayne, Journal of Chemical Physics (2012), 136(15), 154706/1-154706/8

“Atomic Imaging of Atomic H Cleaning of InGaAs and InP for ALD” W. Melitz, J. Shen, T. Kent, R. Droopad, P. Hurley, and A. C. Kummel. ECS Transactions 35 (4), 175-189 (2010).

“InGaAs surface preparation for atomic layer deposition by hydrogen cleaning and improvement with high temperature anneal” W. Melitz, J. Shen, T. Kent, A. C. Kummel, and R. Droopad. Journal of Applied Physics 110, 013713 (2011)

“A Low Band Gap, Solution Processable Oligothiophene with a Dialkylated Diketopyrrolopyrrole Chromophore for Use in Bulk Heterojunction Solar Cells,”Arnold Bernarte Tamayo, Xuan-Dang Dang, Bright Walker, Junghwa Seo, Tyler Kent, and Thuc-Quyen Nguyen, *Appl. Phys. Lett.* 2009, *94,* 103301.

“Influence of Alkyl Substituents and Thermal Annealing on the Performance Solution Processed, Small Molecule- Based Heterojunction Solar Cells,” Arnold Bernarte Tamayo, Tyler Kent and Thuc-Quyen Nguyen, *Energy and Environ. Sci.* 2009, DOI: *10.1039/b912824g.*

“Design, Synthesis, and self-assembly of diketopyrrolopyrrolo derivatives for fabrication of reproducible bulk heterojunction solar cells,” A.B. Tamayo, B. Walker, X. Dang, T. Kent, T.Q. Nguyen, J. Seo. Abstracts of Papers, 238th ACS National Meeting, Washington DC, United States, 2009 PMSE-424

FIELD OF STUDY

Major Field: Materials Science and Engineering

Studies in Surface Science and Physical Chemistry
Professor Andrew C. Kummel

ABSTRACT OF THE DISSERTATION

Passivation of Interface Defects on GaAs and InGaAs (001) and (110) Surfaces and Improvement of Low Temperature HfO_2 ALD Nucleation

by

Tyler James Kent

Doctor of Philosophy in Materials Science and Engineering

University of California, San Diego, 2015

Professor Andrew C. Kummel, Chair

Two obstacles facing the widespread commercial implementation of III-V semiconductors for use as the channel in MOSFETs are the large density of interface trap states at the III-V/oxide interface and challenges associated with deposition of high-k materials for use as the gate oxide on III-V surfaces. Interface trap states are physical defects at the semiconductor-oxide interface that result in electronic band gap states. These defects states typically arise from metallic bonds, bond angle strain, undercoordinated atoms, or contamination on the semiconductor surface.

Additionally modern MOSFETs use tri-gate, or finFET, architectures which usually utilize orthogonal crystallographic planes, such as the (001) and (110) faces, simultaneously. It is crucial to develop methods to clean and passivate both of these crystal faces to allow for high nucleation, aggressive EOT scaling, and low D_{it} of the high-k oxide.

In this work passivation methods for both InGaAs and GaAs (001) and (110) surfaces were developed. STM was utilized to characterize the atomic bonding configuration of the passivants on both the (001) and (110) surfaces, STS was used to characterize the density of states of the passivants, and XPS was used to determine the elemental composition and oxidation states of the surface atoms. It was determined that both surfaces contain inherent defects which can be passivated initially with a reductant, TMA. But chemisorption of TMA on these surfaces creates, directly or indirectly, CB band edge states which can be passivated by a small dose of oxidant.

Ex situ and *in situ* native oxide removal and surface cleaning techniques were examined on the (001) and (110) surfaces. The *ex situ* wet BOE preferentially etched the (001) compared to the (110) surface. An *in situ* surface clean, developed by Carter et al. and Chobpattana et al. for the (001) surface, was found to also be effective on the (110) surface which is ideal when depositing HfO_2 on 3D InGaAs structures. H plasma induced etch damage resulted in a large D_{it} but by including TMA in the surface clean this etch damage was prevented. CV meaurments were made to correlate observations made with STM and STS to electrical device data.

Chapter 1

Introduction

1.1 Trap States at the Semiconductor/Oxide Interface

Fabrication of metal oxide semiconductor field effect transistors (MOSFETs) relies on utilizing atomic layer deposition (ALD) to deposit an oxide layer on a semiconductor surface. Traditional MOSFETs utilized Si as the semiconducting channel material and SiO_2 as the gate oxide. The interface between these two materials is nearly ideal since the native oxide is simultaneously used as the gate dielectric.[1] Si based MOSFETs have reached their physical scaling limit and thus new materials must be employed for both the channel and gate oxide in order to continue improving device performance while minimizing gate leakage.[2] This dissertation investigates InGaAs and GaAs (001) and (110) surfaces for use as the channel, and high-k dielectrics, specifically, Al_2O_3 and HfO_2 for use as the gate oxide.

A major issue facing state of the art MOSFETs based on III-V semiconductors and high-k dielectrics is the semiconductor/oxide interface. These interfaces are plagued with a large density of electronic trap states which result from physical imperfections in the bonding between the semiconductor atoms and the oxide atoms.[3, 4] Although the electronic signatures of interface trap states are well known from capacitance voltage (CV) measurements, the physical origin of these states is still debated.[5-8] This goal of this dissertation to identify the physical origins of the

electronic defects and to develop passivation methods which will lead to a pristine semiconductor/oxide interface and will maximize the nucleation density of the ALD precursors on the InGaAs and GaAs (001) and (110) surfaces.

1.2 Ultra High Vacuum Chamber

All of the x-ray photoelectron spectroscopy (XPS), scanning tunneling microscopy (STM), and scanning tunneling spectroscopy (STS) experiments were performed in an Omicron variable temperature ultra-high vacuum (UHV) chamber. Sample dosing prior to XPS, STM, or STS was performed in a custom built differentially pumped three chamber system comprised of an oxidant dosing chamber, a reductant dosing chamber, and a load lock. The three chamber dosing system had two separate pyrolitic boron nitride (PBN) heaters for dosing at elevated sample temperatures and was differentially pumped by two turbo molecular pumps each backed by a rotary vane mechanical pump. This three chamber system allows for the study of half cycle ALD reactions and provides an entirely *in situ* dosing and characterization environment to prevent contamination of the surface before analysis. After bake out of the dosing chambers a base pressure of $<1 \times 10^{-7}$ torr is achieved. Typically the oxidants used were H_2O, O_2, or H_2O_2 and the reductant used was 98% Trimethylaluminum (TMA) from Strem Chemicals. The preparation chamber has a base pressure of $<1 \times 10^{-10}$ torr and is comprised of an Omicron monochromatic XPS, a low energy electron diffractometer (LEED), a Physical Electronics 10-155 Auger spectrometer, a Stanford Research mass spectrometer, an Oxford Research TC-50

thermal gas cracker, and a tungsten wire for STM tip cracking. The scanning probe microscopy (SPM) chamber consists of an Omicron variable temperature STM and an atomic force microscope (AFM). The base pressure of the SPM chamber is 1 x 10^{-11} torr. A diagram of the chamber is shown in Figure. 1.2.1.

1.3 Scanning Tunneling Microscopy

A large portion of this dissertation utilized STM to determine the surface morphology of various semiconductor surfaces before and after deposition of various half cycle ALD precursors. STM is a technique developed by Binning and Rohrer in 1981. Its operation relies on raster scanning a metallic tip, typically tungsten, with a piezo electric crystal over the surface of interest while applying a bias to the tip relative to the sample and measuring the resulting quantum mechanical tunneling current. The tunneling is exponentially proportional to distance, thus, using a feedback loop to maintain a constant tunneling current, typically 100 picoamperes (pA), causes the tip to move closer or further from the surface which allows for high resolution, on the order of Angstroms (Å), mapping of the surface morphology.[9]

Depending on if the sample is biased positively or negatively relative to the tip different electronic states of the sample will be probed. For example, the GaAs (110) surface is comprised of As atoms with filled dangling bonds and Ga atoms with empty dangling bonds. If the sample is biased negatively relative to the tip then electrons will tunnel from the occupied orbitals of the surface As atoms to the tip since the Fermi level (E_f) of the tip would be located below the valence band (VB) of the

sample, i.e. filled state imaging. If the sample is biased positively relative to the tip then electrons will tunnel from the tip to the sample since the E_f of the tip would be above the conduction band (CB) of the sample, i.e. empty state imaging. In the former case the filled dangling bonds on the As atoms will be directly observed whereas in the latter case the empty dangling bonds of the Ga atoms will be directly observed, figure 1.3.1. The effect of sample bias on tunneling can also provide useful information about the surface density of states (DOS) which can be characterized using STS.

1.4 Scanning Tunneling Spectroscopy

It is possible to obtain information about the local DOS of the surface by placing the STM tip above a single point on the surface and sweeping the sample bias from negative to positive while simultaneously moving the tip towards then away from the surface, i.e. variable height mode. Doing so while recording the current (I) vs. voltage (V) curve and using a lock-in technique to extract the differential conductance (dI/dV) results in an increased dynamic range of several orders of magnitude without increasing acquisition time. Plotting the differential conductance over the normalized conductance results in a plot which is proportional to the DOS of the surface.

$$(dI/dV)/\overline{(I/V)} \propto DOS_{sample}\,(E_f - eV) \qquad (1.4.)$$

Utilizing this technique it is possible to observe electronic states within 4 eV of the E_f and also determine whether or not the E_f is unpinned. The E_f is defined as the 0 V position so for an n-type sample the E_f is expected to be close to the CB edge, while for a p-type sample it should be close to the VB edge. If these cases are not satisfied the E_f is pinned.[10-12]

1.5 X-Ray Photoelectron Spectroscopy

XPS is a surface sensitive spectroscopic technique that relies on irradiating the surface of interest with monochromatic x-rays and measuring the number and kinetic energies of the emitted electrons with a hemispherical analyzer. Each element will eject electrons with specific kinetic energies depending on the core level and orbital thus allowing for determination of the chemical composition of the surface. Additionally, if a certain atom is bonded to a more electronegative or electropositive atom, a chemical shift will be observed in which the characteristic peak for that element will shift at most a few eV giving information about the oxidation state of that atom, hence bonding configuration. Binding energies of the electrons can be extracted since the kinetic energy (KE) of the electron is equal to the characteristic energy of the x-ray photon (hυ) minus the binding energy (BE) of the atomic orbital from which the electron was ejected minus the work function of the spectrometer (Φ_{spec}).[13, 14]

$$KE = h\upsilon - BE - \Phi spec \qquad (1.5.)$$

1.6 Capacitance Voltage Measurements

Performing CV measurements on metal oxide semiconductor capacitors (MOSCAPs) allows for qualitative and quantitative determination of the density of trap states at the semiconductor oxide interface and border traps in the oxide. A typical MOSCAP structure is depicted in Fig. 1.6.1. CV measurements are obtained by sweeping a DC bias between the gate electrode and the backside contact and making AC measurements with frequencies typically ranging from 1 kHz to 1 MHz using an LCR meter. In this dissertation three main characteristics of CV curves are analyzed; the frequency dispersion in accumulation, the magnitude of the false inversion bump, and the maximum capacitance (C_{max}) which is typically a function of oxide quality and thickness. For an n-type sample as you sweep from positive to negative gate biases you initially probe the accumulation region in which the majority charge carriers, electrons, are accumulated at the channel surface. The frequency dispersion throughout the accumulation region can provide information on the border trap densities.[15] As the gate bias approaches zero you pass through the depletion region where the threshold voltage (V_{th}) can be determined. Biasing the gate more negatively leads to the inversion region in which the minority carriers, holes, are accumulated at the channel surface. In the inversion region information can be extracted on the density of interfacial trap states since a large density of trap states will lead to false inversion.[6, 16]

1.7 Density Functional Theory

Density functional theory (DFT) is currently the most accurate quantum mechanical technique to model the electronic structures of many body three dimensional materials.[17] In this dissertation, after observing high resolution STM images, various models for the bonding configurations of ALD precursor chemisorbates on InGaAs and GaAs (001) and (110) surfaces are hypothesized and DFT is used to determine the most thermodynamically favorable structure. Additionally, DFT is utilized to model the DOS of chemisorbates and defects on InGaAs and GaAs (001) and (110) surfaces. By visualizing the band decomposed charge densities it is possible to attribute certain electronic states in the DOS plots to specific physical anomalies on the surface.

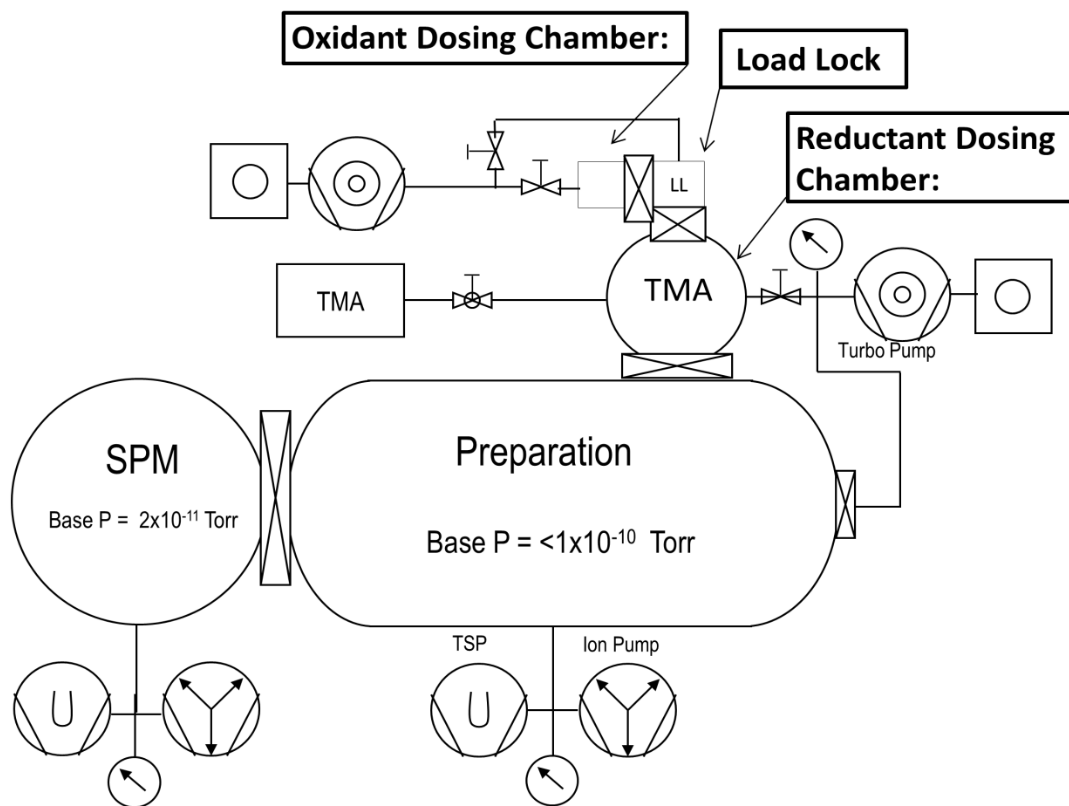

Figure 1.2. Schematic diagram of the Omicron variable temperature UHV system with custom built three chamber dosing system.

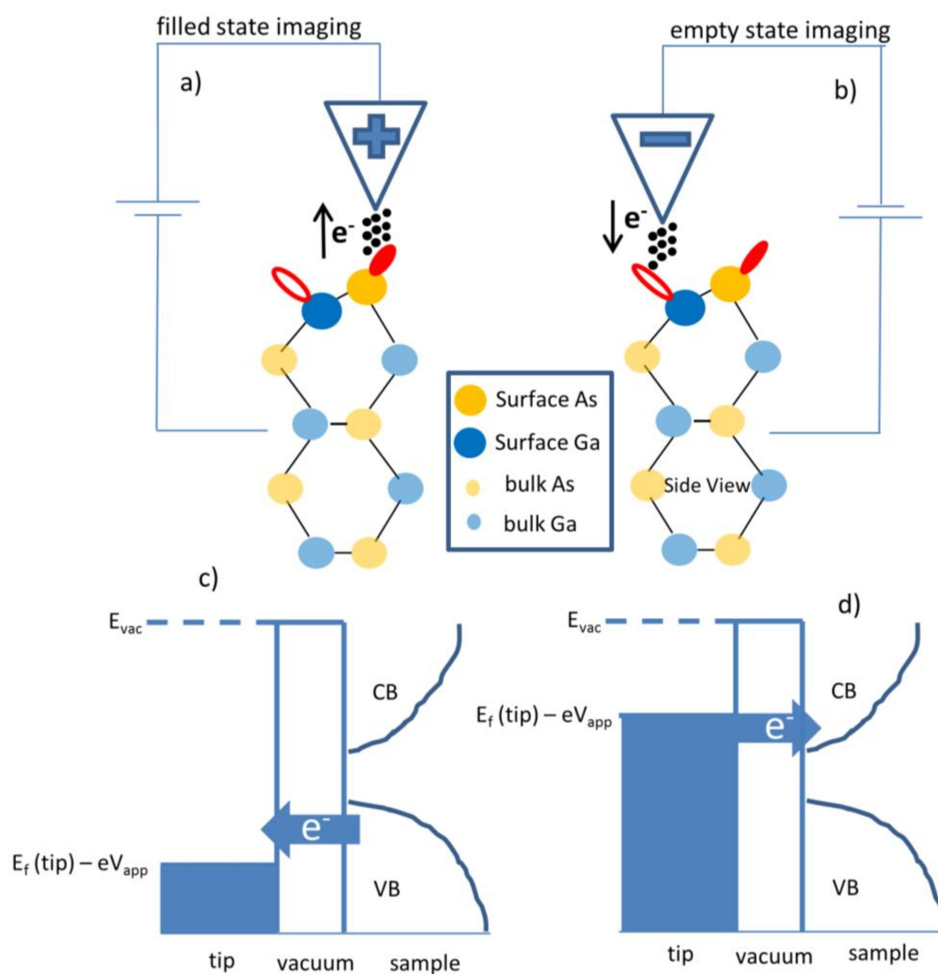

Figure 1.3. a) Schematic representation of filled state STM imaging. b) schematic of empty state STM imaging. c) band diagram of filled state imaging. d) band diagram of empty state imaging

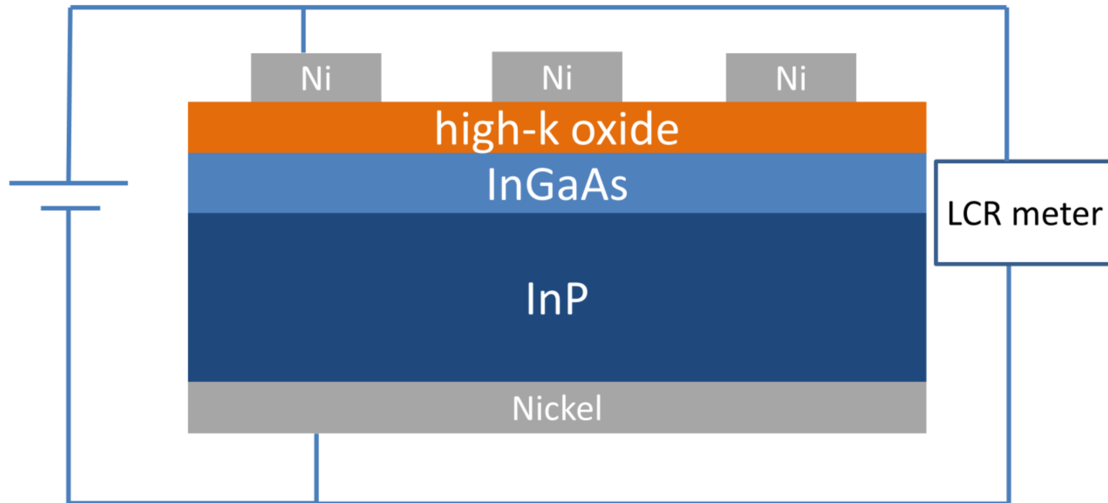

Figure 1.6. Schematic diagram of MOSCAP structure with InGaAs channel, high-k gate oxide, nickel gate contacts, and nickel backside contact. A DC bias is swept between gate and backside contact and simultaneously an LCR meter is used to measure the frequency dependent capacitance response.

1.8 References

[1] E. H. Nicollian, J. R. Brews, and E. H. Nicollian, *MOS (metal oxide semiconductor) physics and technology* (Wiley New York et al., 1982).

[2] M. M. Heyns, Solid State Phenomena **187**, 3 (2012).

[3] P. D. Ye, Journal of Vacuum Science & Technology A: Vacuum, Surfaces, and Films **26**, 697 (2008).

[4] W. Mönch, *Semiconductor surfaces and interfaces* (Springer, 2001).

[5] H.-C. Lin, W.-E. Wang, G. Brammertz, M. Meuris, and M. Heyns, Microelectronic Engineering **86**, 1554 (2009).

[6] R. Engel-Herbert, Y. Hwang, and S. Stemmer, Journal of Applied Physics **108**, 124101 (2010).

[7] H. Hasegawa and H. Ohno, Journal of Vacuum Science & Technology B **4**, 1130 (1986).

[8] J. Robertson, Applied Physics Letters **94**, 152104 (2009).

[9] G. Binnig and H. Rohrer, Surface science **126**, 236 (1983).

[10] R. M. Feenstra, Surface science **299**, 965 (1994).

[11] J. A. Stroscio, R. Feenstra, D. Newns, and A. Fein, Journal of Vacuum Science & Technology A: Vacuum, Surfaces, and Films **6**, 499 (1988).

[12] R. M. Feenstra, G. Meyer, F. Moresco, and K. H. Rieder, Physical Review B **66**, 165204 (2002).

[13] D. Briggs and M. P. Seah, D. Briggs, & M. P. Seah,(Editors), John Wiley & Sons, Chichester 1983, xiv+ 533 (1983).

[14] J. M. Hollander and W. L. Jolly, Accounts of Chemical Research **3**, 193 (1970).

[15] D. Fleetwood, M. Shaneyfelt, W. Warren, J. Schwank, T. Meisenheimer, and P. Winokur, Microelectronics Reliability **35**, 403 (1995).

[16] T. D. Lin, Y. H. Chang, C. A. Lin, M. L. Huang, W. C. Lee, J. Kwo, and M. Hong, Applied Physics Letters **100** (2012).

[17] E. A. Chagarov and A. C. Kummel, in *Fundamentals of III-V Semiconductor MOSFETs* (Springer, 2010), p. 93.

Chapter 2

Dual Passivation of Intrinsic Defects at the Compound Semiconductor/Oxide Interface Using an Oxidant and a Reductant

2.1 Abstract

Studies have shown that metal oxide semiconductor field-effect transistors fabricated utilizing compound semiconductors as the channel are limited in their electrical performance. This is attributed to imperfections at the semiconductor/oxide interface which cause electronic trap states, resulting in inefficient modulation of the Fermi level. The physical origin of these states is still debated mainly because of the difficulty in assigning a particular electronic state to a specific physical defect. To gain insight into the exact source of the electronic trap states, density functional theory was employed to model the intrinsic physical defects on the InGaAs (2x4) surface and to model the effective passivation of these defects by utilizing both an oxidant and reductant to eliminate metallic bonds and dangling-bond-induced strain at the interface. Scanning tunneling microscopy and spectroscopy were employed to experimentally determine the physical and electronic defects and to verify the effectiveness of dual passivation with an oxidant and a reductant. While subsurface chemisorption of oxidants on compound semiconductor substrates can be detrimental, it has been shown theoretically and experimentally that oxidants are critical to removing metallic defects at oxide/compound semiconductor interfaces present in nanoscale channels, oxides, and other nanostructures.

2.2 Introduction

Traditional MOSFETs utilized Si as the channel material, but in an effort to increase processing power in logic devices compound semiconductors are being explored as an alternative channel due to their intrinsically high mobilities.[18, 19] Studies over the past several decades have concluded that a limiting factor to compound semiconductor based MOSFET performance is the large density of interface trap states at the semiconductor/oxide interface.[4, 20-23] These electronic trap states are hypothesized to be a result of physical imperfections at the semiconductor/oxide interface such as dangling bonds, highly strained bond angles, and metallic bonds, although this is still a topic of debate.[3, 8] In order to develop effective passivation techniques for compound semiconductor/oxide interfaces it is critical to definitively identify the physical origin of these electronic trap states. Previous work has shown that the deposition of a-Al_2O_3 on the InGaAs (2x4) surface results in promising CV characteristics.[24] Therefore, the As-rich (2x4) reconstruction of InGaAs is a viable choice for use as a surface channel, but there is a fundamental problem with this surface for alloy compositions ranging from InAs to GaAs.

Edmonds et al. showed that GaAs (2x4) or InAs (2x4) surfaces contain at least 8% α2-(2x4) unit cells and In0$_{.53}$Ga$_{0.47}$As contains 71% α2-(2x4) unit cells which accentuates the need to effectively passivate these defect unit cells.[25] The α2-(2x4) unit cell is missing an As-As dimer on the row which results in metallic In-Ga bonds.[26] The metal-metal bonds directly form VB edge states and indirectly induce CB edge states; the metal-metal bonds generate bond angle strain in the edge As atoms

which prefer to be in a tetrahedral sp^3 bonding configuration. This bond strain results in CB edge states as seen in DFT calculations of the (2x4) surface DOS and prevents the E_f from being efficiently modulated without proper passivation techniques. Therefore, the InGaAs (2x4) reconstruction requires passivation of at least three unique sites: As dangling bonds, In/Ga dangling bonds, and In/Ga-In/Ga bonds.

Many passivation techniques have been explored for compound semiconductor surfaces, but most rely on external wet cleans, chemicals that are not ideal for introduction into commercial ALD tools, or temperatures that are not practical.[27-31] Another option would be to avoid the inherent problems of the InGaAs (2x4) surface by using another crystallographic face such as the (110) surface which is defect free.[12, 32, 33] While pre-dosing with a reductant such as TMA is well known to improve device characteristics and reduce native oxides,[24, 34] the reductant (TMA) can only passivate the dangling bonds on the As atoms since bonding to a metal (Al) cannot passivate either In/Ga dangling bonds nor In/Ga-In/Ga metallic bonds.[35] To improve III-V (2x4) based MOSFET device performance, it may be possible to passivate the high density of defect unit cells using *in situ* chemical processes which preferentially insert an oxidant species such as an –OH group into the metallic bonds and relieve the strained As bonds. In this work, a passivation technique which utilizes a reductant (TMA) and an oxidant (OH, SH, NH_2) to passivate defect unit cells on the InGaAs (001)-(2x4) surface is modeled using DFT and experimentally tested using STM and STS. To determine the chemical mechanism of passivation the order of TMA/oxidant dosing was reversed and two different oxidants were studied.

2.3 Methods

The samples contained 0.2 μm of molecular beam epitaxy (MBE) grown $In_{0.53}Ga_{0.47}As$ (001) with 1 x 10^{18} cm^{-3} Si dopant concentrations on commercially available InP wafers. The samples were capped with ~50 nm of As_2 to protect the InGaAs surface from contaminants and oxidation. Samples were loaded into an Omicron variable temperature-UHV system with a base pressure of <1 x 10^{-10} torr. The As_2 cap was thermally desorbed at 350 ˚C, and the (2x4) surface reconstructions were obtained by annealing the samples to 400 ˚C. Samples were transferred *in situ* to the SPM chamber with a base pressure of 1 x 10^{-11} torr where STM and STS were performed on the clean (2x4) surfaces. STM experiments were performed in constant current mode with a sample bias of -3 V and a tunneling current set point of 100 pA. All images have been reproduced at least twice. The distance between rows was determined by averaging 10 separate line traces and calculating the standard error. STS was performed in varied-z mode while ramping the sample bias from -1.5 to 1.5 V while concurrently moving the tip toward then away from the surface. All STS curves are an average of at least 8 individual curves. After dosing TMA and/or an oxidant, STM was used to determine the atomic configuration of the surface while STS was used to measure the electrical quality of the surface.[4, 10, 11] Specific dosing conditions for each experiment are given in the corresponding results section.

All DFT calculations were performed with the Vienna Ab-Initio Simulation Package (VASP)[36, 37] using projector augmented-wave (PAW) pseudopotentials (PP)[38] and the PBE (Perdew-Burke-Ernzerhof) exchange-correlation functional.[39, 40] The

choice of PBE functional and PAW PPs was validated by parameterization runs demonstrating good reproducibility of experimental lattice constants, bulk moduli, and formation energies for bulk crystalline GaAs and InAs. The three bottom layers of InGaAs were permanently fixed in their bulk-like positions and passivated by pseudo-H atoms with 1.25 |e| charge to simulate continuous bulk. The systems were DFT-relaxed by Conjugate-Gradient (CG) geometry-optimization algorithm with a force tolerance level of 0.05 eV/Å at 4x8x1 Gamma-centered K-point set.

2.4 Results and Discussion

2.4.1 Density Functional Theory Simulations

Fig. 2.1 shows a DFT model of the InGaAs (001) α2-(2x4) defect unit cell with a missing As row dimer which had been passivated with a full monolayer of dimethylaluminum (DMA). In the calculated DOS (c), small VB and CB edge states are observed, pink and purple arrows respectively. The band decomposed charge density, left and middle, shows the origin of these states in the structural models. Fig. 2.1(a) shows the VB edge states (pink lobes) which are predominantly concentrated on the In-Ga metallic bonds. Fig. 2.1(b) shows the CB edge states (purple lobes) originate mainly from the edge sp^3 hybridized As atoms which have a highly strained bond angle of about 65˚ which is much smaller than the ideal tetrahedral angle of 109.5˚

To model the effects of oxidant passivation, calculations were performed for –O-, -S-, and –NH insertion into the metallic group III bonds to eliminate the metal-metal bonds and relieve the strained As bonds. Fig. 2.2 shows the resulting bonding

configurations and calculated DOS after oxidant insertion. The electronic structures for –O-, –S-, and -NH insertion are nearly identical consistent with their isoelectric properties. The –O-, –S-, and -NH insertion reduced the VB edge state by eliminating the In-Ga metallic bonds. However, the edge As atoms still have non-tetrahedral bond angles (red arrows) consistent with negligible reduction in the CB edge state density.

To test if a different bonding angle might influence the CB edge states, DFT was employed to model –OH, -SH, and –NH_2 insertion into the metallic bonds as shown in Fig. 2.3. Note all three ligands give nearly identical electronic structures. These hydride insertion results have a less passivating effect on the VB edge states compared to simple atomic insertion, but there is partial passivation of the CB edge states. The DFT structural model shows the cause of the CB edge state partial passivation. Although pairs of –OH, -SH, and –NH_2 groups were inserted into the metal-metal bonds, DFT relaxation resulted in one of the hydride groups moving out of the metal-metal bond and eliminating a dangling bond of one of the tri-coordinated In/Ga atoms. This configuration satisfies the electron counting model whereas having two bridging oxidant groups or two edge oxidant groups leads to excess charge or a charge deficiency, respectively. The lack of passivation of the VB edge states is consistent with one of the metal-metal bonds remaining intact while the partial passivation of the CB edge state is consistent with the dangling bonds on the tricoordinated In/Ga atoms being a source of the bond angle strain which induced CB edge states. As shown in Fig. 2.1, the empty dangling bonds on the tricoordinated In/Ga atoms do not directly induce CB edge states, instead they induce bond angle

strain on the neighboring As atoms (red arrows) which causes the CB edge states.

To eliminate both the metal-metal bonds and the group III dangling bonds in the DFT model two –OH, -SH, or $–NH_2$ groups were inserted into the metallic bonds and bonded to the edge tricoordinated In/Ga atoms. Note all three ligands give nearly identical electronic structures. One of the methyl groups from the DMA molecule migrated and bonded to the left surface Ga atom. This configuration satisfies the electron counting rule and results in a neutral unit cell. Additionally this double passivation restored the edge As atom bond angles to sp^3 tetrahedral geometry with an angle much closer to the ideal 109.5˚ and the CB edge states were completely suppressed as shown in Fig. 2.4 (b),(c), and (d). The models are consistent with the effect of dual passivation: a reductant (TMA) is used to eliminate the dangling bonds on the tricoordinated As atoms while an oxidant (–OH, -SH, or $–NH_2$) is used to eliminate both the metal-metal bonds and the group III dangling bonds.

2.4.2 STM/STS

After decapping the sample, STM was used to verify the InGaAs (001)-(2x4) surface was free of contaminants, Fig. 2.5(a). The zig-zag pattern of the rows in the STM image is due to the presence of two different unit cells on the (2x4) surface, the α2-(2x4) and the β2-(2x4) unit cells.[26] Details of the different unit cells are given in a previous study which has shown that $In_{0.27}Ga_{0.73}As$ contains 42% missing dimer unit cells and $In_{0.53}Ga_{0.47}As$ has 78%.[25] DFT simulations (Fig. 2.1 - 2.4) show that the defect unit cells cannot be fully passivated by TMA and require an oxidizing agent to

suppress the remaining CB edge states. Two passivation experiments were performed to achieve dual passivation.

In the first experiment 1000 L of HOOH vapor was dosed onto the clean (2x4) surface at 25 ˚C and followed by anneals at 210, 250, 350, and 410 ˚C, each for 30 min. A STM image of the final surface is shown in Fig. 2.5 (b). By manually counting the number of α2-(2x4) unit cells in the STM image, it was determined that the percentage of α2-(2x4) unit cells was decreased from 78% to 24% consistent with selective insertion of –OH groups into the metallic group III bonds. The HOOH dosed InGaAs (001)-(2x4) sample was subsequently annealed to 460 ˚C for an additional 30 min as shown in Fig. 2.5 (c). The characteristic zig-zag pattern of the clean surface is visible indicating the adsorption of –OH is reversible and there is no subsurface oxidation for low temperature dosing even with a high temperature anneal since this would irreversibly change the surface structure. In a separate experiment 3000 L of HOOH was dosed followed by the same series of anneals in an attempt to reduce the number of α2 unit cells. No high resolution images were obtained after several days of scanning. It is believed the oxidant was regularly reacting with the tip, effectively limiting the resolution of the image.

Fig. 2.6 shows a sample that was initially dosed with 1500 L of HOOH, annealed to 320 ˚C, and subsequently dosed with 500 L of TMA at 25 ˚C and annealed to 280 ˚C. The HOOH dosing is manually controlled, hence the variation in total dose between Fig. 2.5 and Fig. 2.6 is limited by the ability to control the extent of manual dosing in real time. There are atomically ordered rows in the $(\bar{1}10)$ direction with

row spacing of 1.68 ± 0.09 nm, the same as the clean (2x4) surface (Fig. 2.6 inset). This suggests the lack of subcutaneous oxidation, but the zig-zag pattern observed for both the clean (2x4) surface and the TMA only dosed surface is not visible indicating preferential insertion of the –OH groups into the metallic bonds.[35] Growth of Al_2O_3 has been nucleated in each unit cell because the TMA selectively reacted with the As-As dimers and the HOOH reacted with the group III bonds.

An STS study was performed to determine the effects of dosing TMA only (green curve), HOOH only (red curve), and dual passivation with HOOH and TMA (pink curve), Fig. 2.7. The E_f, defined as the 0 V position in STS, is located near the CB edge for the clean surface (blue curve) meaning the E_f is unpinned. Previous studies on clean n-type and p-type InGaAs (2x4) and on TMA dosed n and p-type InGaAs (2x4) demonstrated that the E_f remained near the VB for p-type samples and near the CB for n-type samples indicating an unpinned Fermi level.[35] After dosing with 1000 L of TMA (green curve) at 280 ˚C with a 280 ˚C anneal, the E_f shifts slightly towards midgap indicating a partially pinned surface. After dosing the clean (2x4) surface with 1000 L of HOOH (g) (red curve) at 25 ˚C with 310 ˚C anneal, the Fermi level position remains unchanged from the clean surface position, which is in contrast to several publications indicating oxidant dosing of III-V surfaces results in a pinned E_f.[22, 41-43] Dosing 1000 L of HOOH at 25 ˚C with a 300 ˚C anneal and subsequently 1000 L of TMA at 280 ˚C followed by an anneal at 280 ˚C for 30 min (pink) results in further unpinning of the E_f when compared to the TMA only dose. Although the DFT calculations showed that reacting the clean (2x4) surface with both

TMA and –OH groups should passivate CB edge states, this experiment shows that dosing both TMA and HOOH does not completely unpin the Fermi level. To achieve a fully unpinned surface E_f it may be necessary to decrease the number of α2-(2x4) unit cells below 23% by further optimizing the dosing conditions. However, in gate oxide deposition, there will be subsequent exposure to H_2O during ALD which is likely to remove most remaining metal-metal bonds. To ensure the E_f was not pinned near the CB due to In surface segregation[7] n and p-type samples were compared, Fig 2.8. A p-type sample was dosed with 1000 L of HOOH at 25 ˚C and subsequently dosed with 1000 L of TMA at 280 ˚C. The E_f is located near the VB for the p-type sample and near the CB for the n-type sample indicating the E_f is not pinned near the CB.

2.5 Conclusions

This study has identified the physical origins of electronic trap states present at the InGaAs/oxide interfaces and presented an effective dual passivation scheme using an oxidant and a reductant which eliminates metallic bonds, dangling bonds, and dangling bond induced strain. Employing this passivation technique will result in superior electrical performance due to suppression of electronic defects and is applicable to a wide range of devices containing a compound semiconductor/oxide junctions.

2.6 Acknowledgments

This work was supported by the semiconductor research corporation (SRC). Chapter 2 is in part or full, reprinted with permission from T. Kent, E. Chagarov, M. Edmonds, R. Droopad, and A. C. Kummel, "Dual Passivation of Intrinsic Defects at the Compound Semiconductor/Oxide Interface Using an Oxidant and a Reductant." ACS nano (2015). The dissertation/thesis author was the primary investigator and author of this paper.

2.7 Supplemental Material

A second dual passivation method was studied. TMA was dosed first using the same procedure mentioned in the article. Following TMA deposition, 150,000 L of H_2O was dosed at 80 ˚C and subsequently annealed to 100 ˚C for 30 min. Fig. 2.9 (a) shows an STM image of the resulting surface which is atomically flat and has ordered rows in the $(\bar{1}10)$ direction with 1.72 ± 0.04 nm spacing (inset). This suggests the –OH groups inserted into the In-Ga metallic bonds without displacing any DMA molecules. STS in Fig. 2.9 (b) shows that the E_f shifted towards the CB after dosing with H_2O at 80 ˚C consistent with passivation of the CB edge states as suggested by DFT simulations and a fully unpinned E_f. In a separate experiment, water was dosed at 120 ˚C and Fig. 2.9 (b) shows the STS spectra obtained. In contrast to the 80 ˚C dose the Fermi level did not shift. Results from the McIntyre group also suggest dosing water at 80 ˚C gives optimal CV characteristics compared to higher and lower oxidant dosing temperatures.[44] It is noted that in the STS measurements, the

magnitude of the normalized conductance can vary significantly while the E_f position relative to the band edges is more stable. Among 25 different STS curves, the average magnitude and standard deviation of the differential conductance was 0.61 ± 0.66 nA/V. This indicates no meaningful conclusions can be drawn about the total VB or CB DOS from our results. On the other hand the average E_f position relative to the VB for the 80 ˚C H_2O dose was 0.76 ± 0.07 V and 0.35 ± 0.09 V relative to the CB with standard errors of 0.02 and 0.04 respectively. This suggests that averaging at least 10 curves gives an accurate E_f position and any fluctuation is not a result of varying In concentrations but rather a direct result of processing conditions. Additionally STS was performed on a p-type sample which was dosed with TMA and subsequently water, Fig. 2.10. For the p-type sample the E_f is located near the VB edge state whereas for the n-type sample the E_f is located near the CB edge indicating it is fully unpinned.

Figure 2.11 demonstrates the difference between the bulk InGaAs calculated DOS vs. the (2x4) surface DOS. The image shows an InGaAs bulk supercell passivated with H_2 on the top and the bottom layers (top). This is necessary to obtain the same quantum confinement effects that are observed when simulating the (2x4) surface. Comparing the calculated DOS (bottom) the bulk CB edge (red curve) starts at 0.5 eV whereas the CB edge for the (2x4) surface (black curve) starts at 0.3 eV. These surface states result from defect unit cells that cannot be passivated by TMA alone but require both an oxidant and reductant. More details on the inherent defects on the (2x4) surface can be found elsewhere.[25]

In order to determine the effect of In/Ga distribution in the DFT simulations, a defect unit cell with a random distribution of In and Ga was modeled, Fig. 2.12. The clean defect unit cell shows that the CB edge state has shifted toward midgap, compared to the ordered unit cell.[25] After passivation with TMA the midgap state is passivated and shifted toward the CB. Although the bandgap is slightly narrower than the ordered unit cell the semi-passivating effect of the TMA is still observed. As in the case of the ordered unit cell, the CB edge state persists due to the strained As bonds adjacent to the metallic In/Ga surface bonds (red arrow). Full passivation is achieved with additional oxidation of the metallic bonds.

An additional structure of possible importance is shown in Fig. 2.13. In this case O atoms or S atoms were inserted into the metallic bonds while –OH and –SH groups were bonded to the edge In/Ga atoms. Such a structure could be obtained by the recombinative desorption of H_2 leaving behind an O or S atom in the bridging position. In the case of the O atom, the calculated DOS shows a large amount of VB states. This system does not satisfy the electron counting rule, which explains the poor electronic structure. In the case of the S atom insertion the bandgap looks clean with no VB or CB states. This is a result of migration of one of the –SH groups from the edge Ga atom onto the S atom. In this configuration the electron counting rule is satisfied. A small CB edge state remains due to incomplete relaxation of the strained As edge atom (red arrow).

The most efficient passivating configuration, Fig. 4, was modeled with an In rich surface layer to determine the effect on the DOS, Fig. 2.14. Fig. 2.14 (a) shows

the TMA passivated α2 unit cell. The CB state onset is shifted about +0.1 eV compared to the 50% In/Ga case. For the –OH and -SH passivating cases (b) and (c) respectively, the CB edge state onset is shifted about +0.05 eV. For the $–NH_2$ case (d) there is no difference between the In rich case and the 50% In/Ga case. These results indicate that In surface segregation does not have a significant impact on the system. The presence of CB edge states is primarily attributed to the inherent defects of the (2x4) surface and that passivation of these defects is primarily due to selective insertion of an oxidant and a reductant into each unit cell.

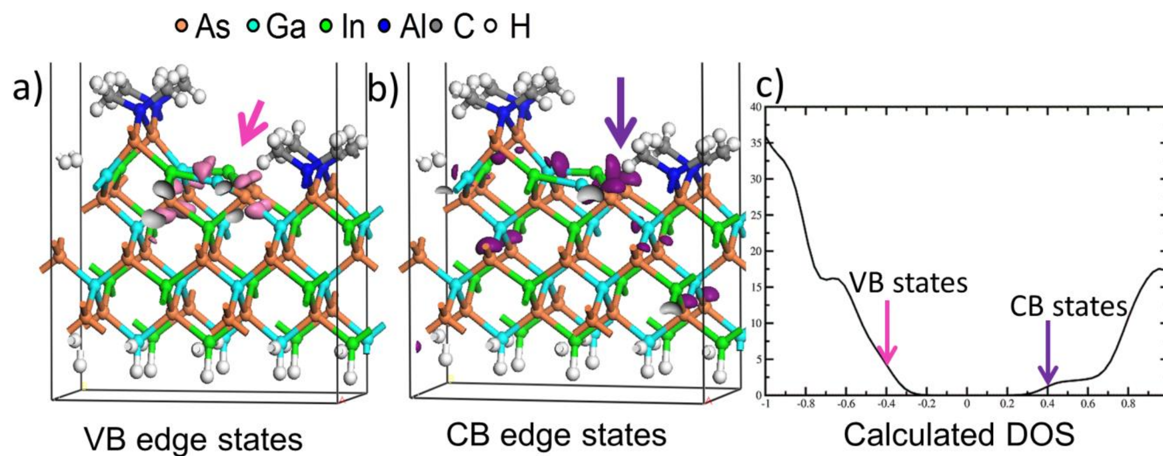

Figure 2.1. (a) side view of relaxed DFT models of TMA passivated α2-(2x4) unit cell with pink lobes showing origin of VB edge states. (b) purple lobes showing origin of CB edge states. (c) density of states of TMA passivated α2-(2x4) unit cell with arrows indicating the band edge states.

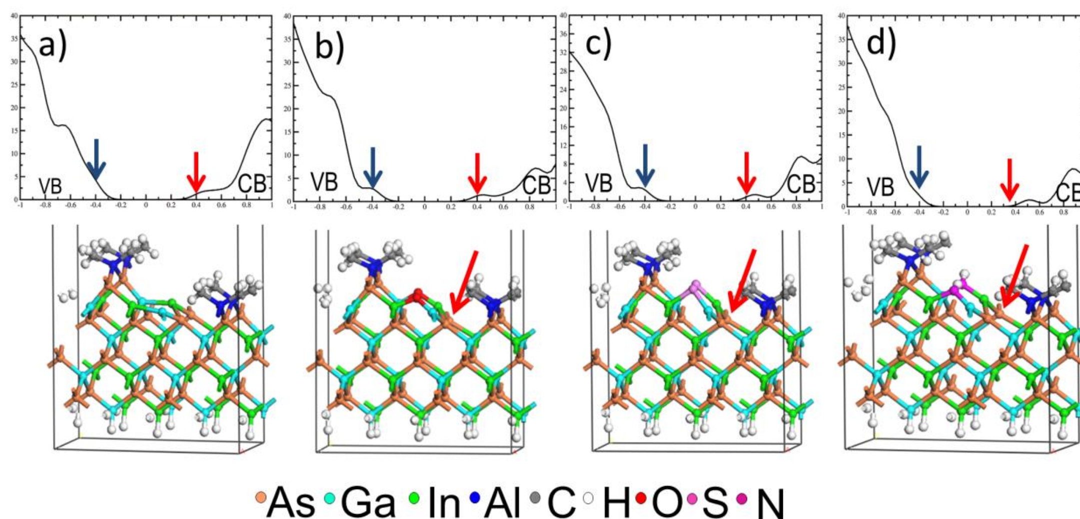

Figure 2.2. Side view of relaxed DFT models and DOS of TMA passivated (2x4) surface (a) with an O atom (b), S atom (c), and -NH atom (d) inserted between group III atoms. Note the electronic structures for passivation with O and S are nearly identical. Both reduce the VB edge state by eliminating the In-Ga metallic bonds. However, the edge As atoms (arrow) still have non-tetrahedral bond angles. The N passivation leaves the edge As atoms with highly distorted bond angles (arrow) and ½ filled dangling bonds on N atoms which pin the Fermi level.

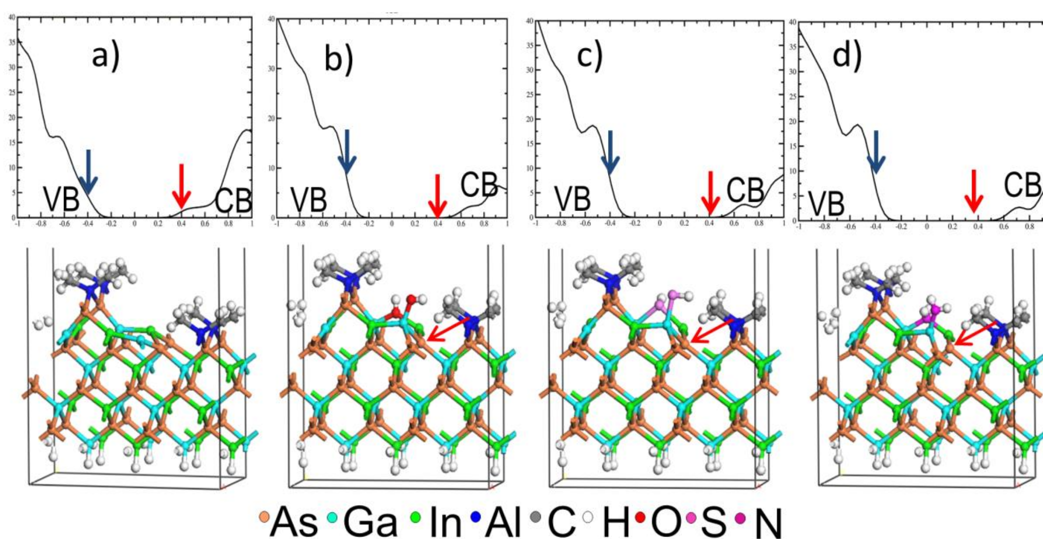

Figure 2.3. Side view of relaxed DFT models and DOS of TMA passivated (2x4) surface (a) with an -OH group (b), -SH group (c), and –NH_2 group (d) inserted between group III atoms. Note the electronic structures for passivation with -OH, -SH, and -NH_2 are nearly identical. In all cases, half of the ligands migrated out of the In-Ga bonds to passivate a Ga dangling bond resulting in an increase of VB edge states and a decrease of CB edge states. All cases reduced the CB edge state by eliminating the In-Ga metallic bonds and partially relieving bond angle strain in the edge As atoms.

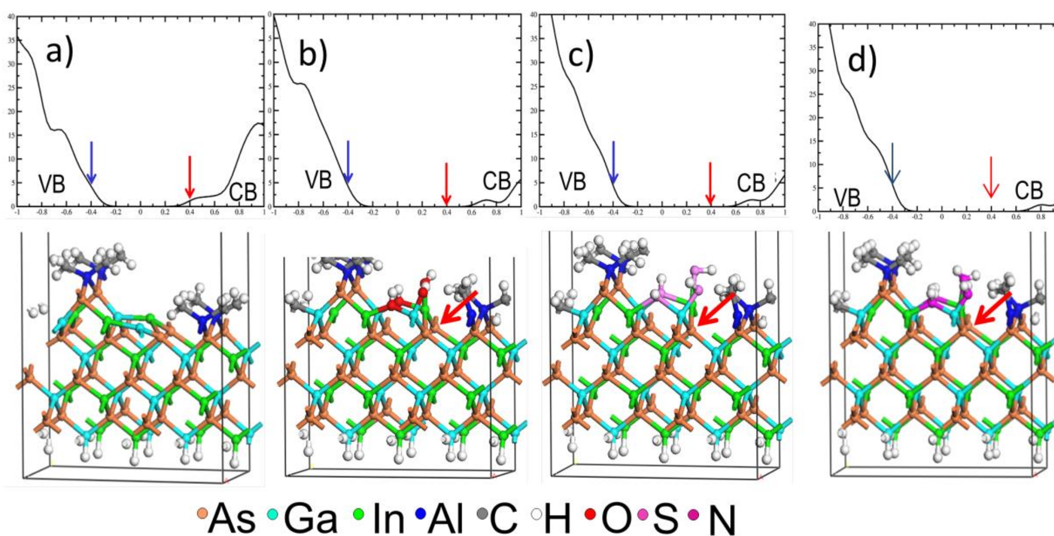

Figure 2.4. Side view of relaxed DFT models and DOS of TMA passivated (2x4) surface (a) with two -OH groups (b), -SH groups (c), -NH_2 groups (d) inserted between group III atoms and on the edge group III atoms. The electronic structures for passivation with -OH, -SH, and -NH_2 are nearly identical. The ligands have removed the dangling bonds on the In and Ga atoms resulting in the edge As atoms (arrows) being restored to bulk-like tetrahedral bonding angles which eliminates the CB edge states.

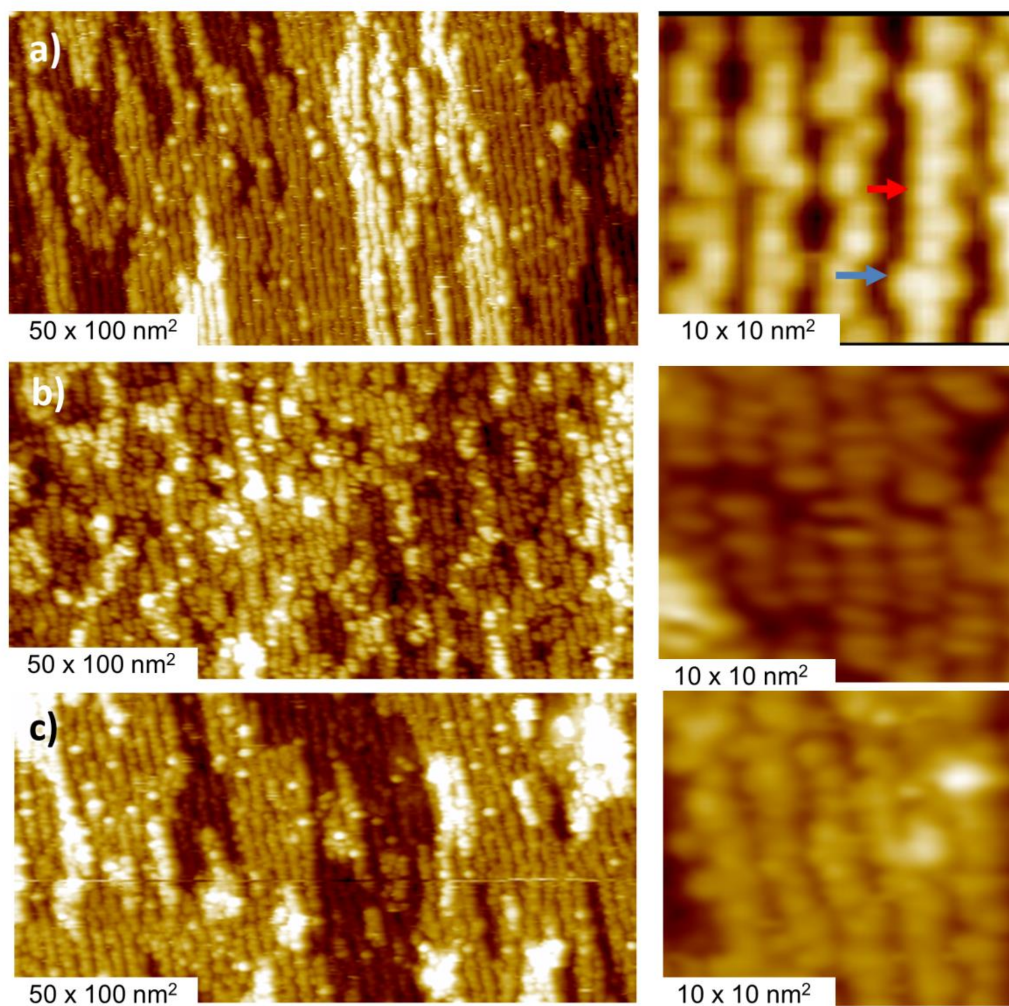

Figure 2.5. (a) filled state STM images of clean (2x4) surface with β2 double As dimer unit cell (blue arrow) and α2 single As dimer unit cell (red arrow) (b) 1000 L dose of HOOH followed by a series of anneals, notice majority of unit cells appear wide indicating selective insertion of –OH groups into metallic In-Ga bond (c) same sample after annealing up to 460 ˚C, notice restoration of characteristic zig-zag pattern indicating reversible chemisorption of –OH groups on (2x4) surface.

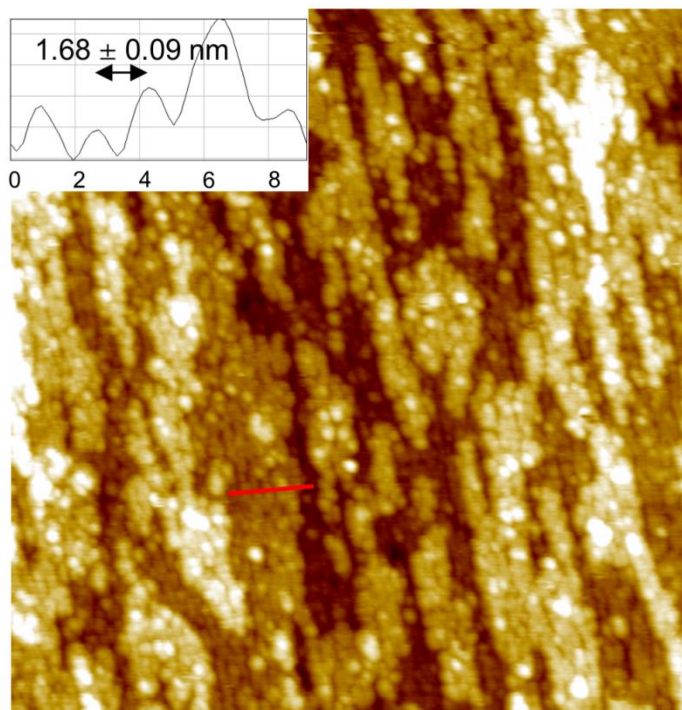

Figure 2.6. 100 x 100 nm^2 filled state STM image of the InGaAs (2x4) surface initially dosed with HOOH and subsequently dosed with TMA. Ordered rows appear in vertical direction indicating high degree of surface order is maintained (inset) but the zig zag pattern of typical (2x4) surface is not observed indicating selective insertion of –OH groups into metallic In-Ga bonds. Al_2O_3 ALD is nucleated in each unit cell since TMA reacted with As dimers and –OH groups reacted with In/Ga atoms.

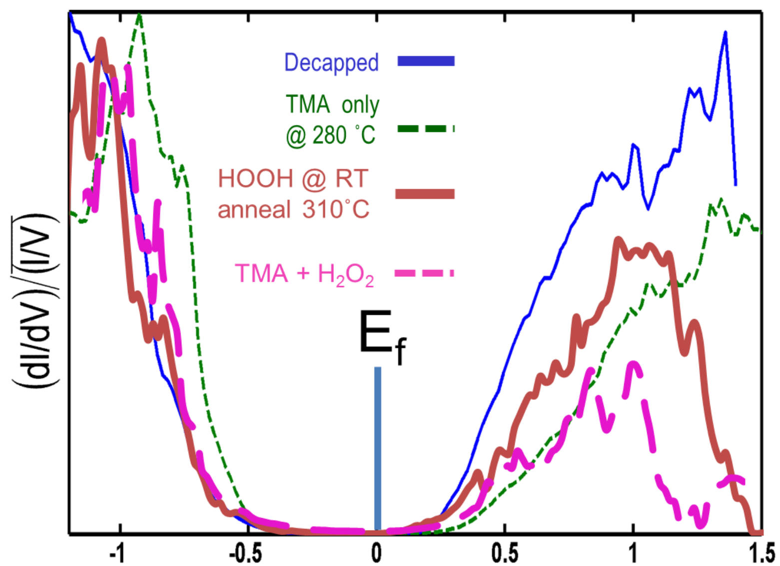

Figure 2.7. STS spectra of the clean (2x4) surface (blue) showing Fermi level near CB edge indicating unpinned Fermi level, the TMA dosed surface (green) which shows slight shift of Fermi level towards midgap due to unpassivated metallic bonds, the HOOH dosed surface (red) which is nearly identical to clean surface, and the TMA + HOOH dosed surface (pink) which has Fermi level near CB edge consistent with unpinning

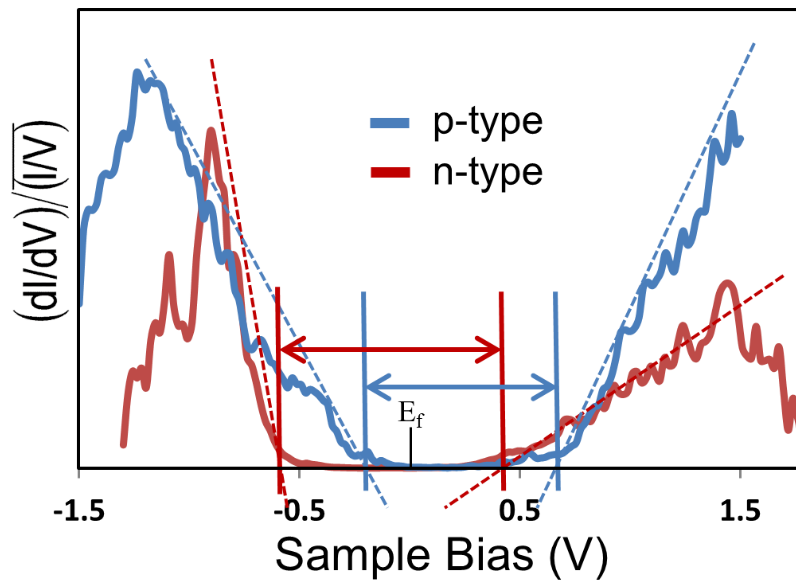

Figure 2.8. STS of n (red curve) and p-type (blue curve) InGaAs dosed with 1000 L of HOOH followed by 1000 L of TMA. To ensure the E_f is fully unpinned p-type InGaAs was dosed and the E_f is clearly located near VB for p-type sample indicative of unpinning.

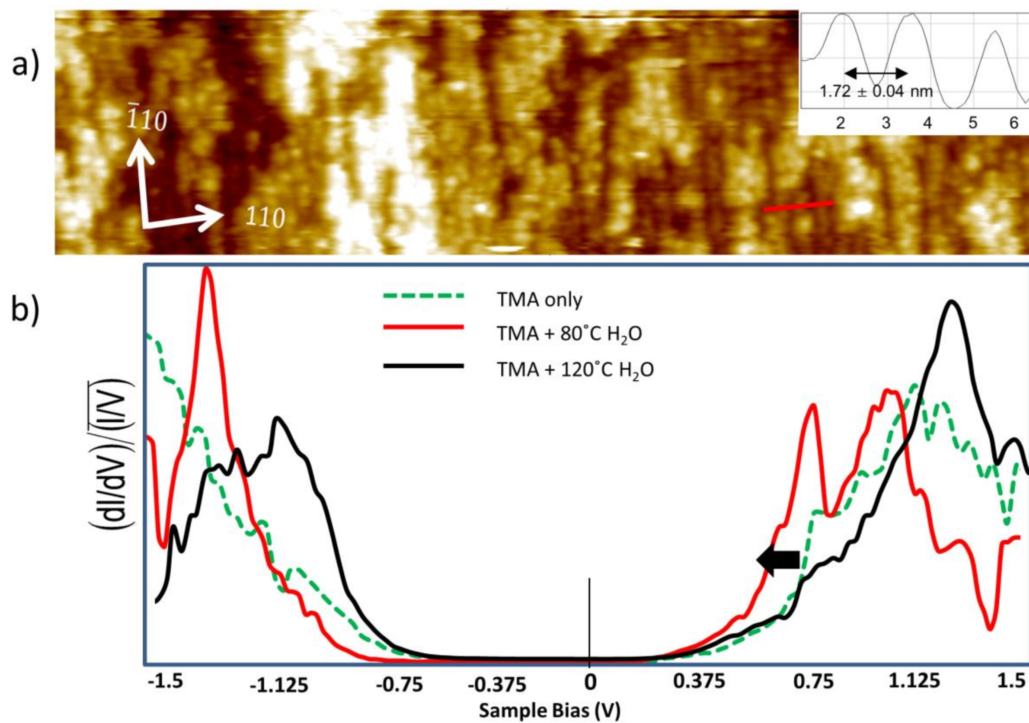

Figure 2.9. (a) 20 x 100 nm^2 filled state STM image of the TMA+H_2O dosed surface. Surface maintains high degree of order (inset) with 1.72 nm between adjacent rows. (b) STS spectra of TMA dosed surface (green) **,** 80 ˚C H_2O + TMA dosed surface (red) showing 80 ˚C water pulse further unpins Fermi level, and 120 ˚C H_2O + TMA surface (black) showing no Fermi level shift.

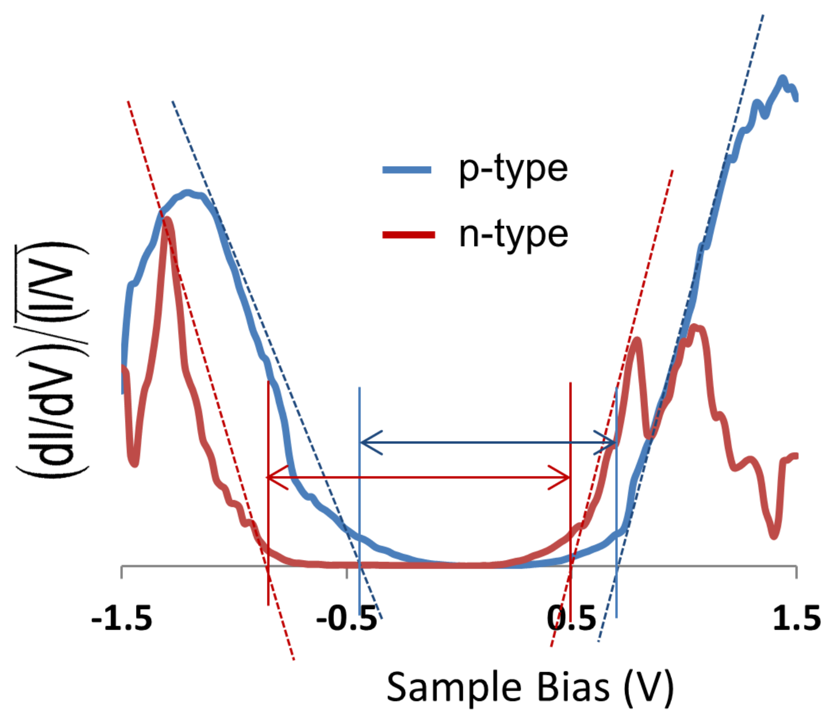

Figure 2.10. n-type (red) and p-type (blue) sample initially dosed with TMA and then H_2O using same conditions as Fig.9. E_f for p-type sample is located near the VB while E_f for n-type sample is near the CB indicating it is unpinned.

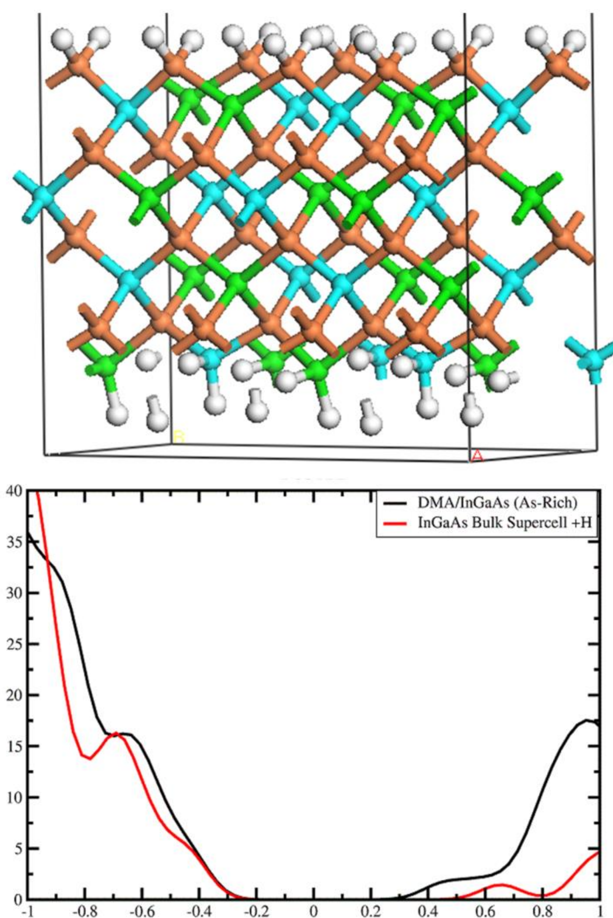

Figure. 2.11 (top) DFT model of InGaAs bulk supercell passivated with H_2 on top and bottom of the cell. This is necessary to obtain the same quantum confinement effects as the other simulations. (bottom) calculated DOS of the DMA/InGaAs (2x4) unit cell (black line) and InGaAs bulk supercell (red line). Notice the (2x4) surface has conduction band states beginning at 0.3 eV whereas the bulk bandgap lacks CB states. As described in the paper these CB edge states can be partially passivated with TMA and fully passivated with TMA and an oxidant.

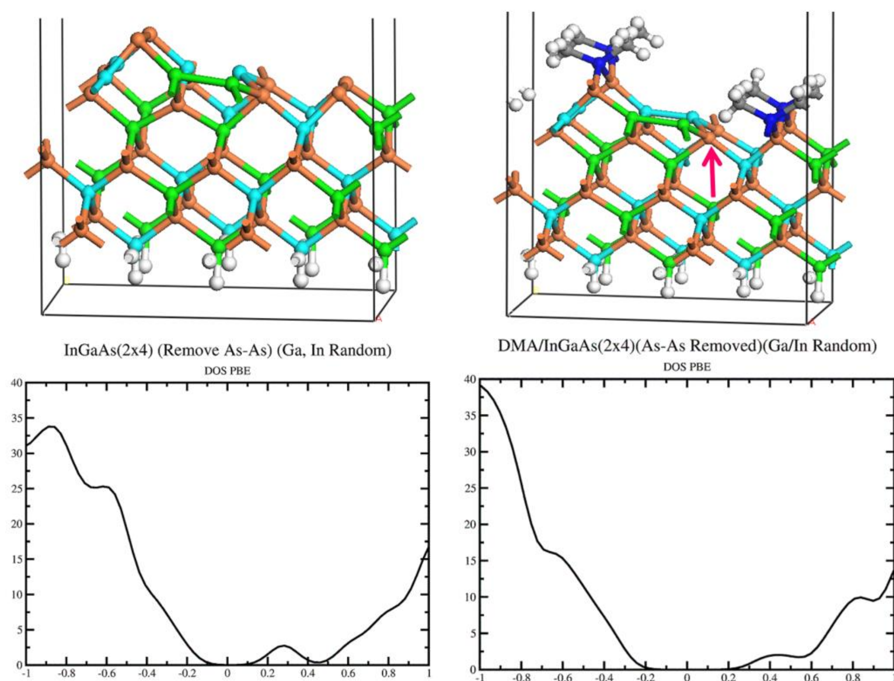

Figure 2.12. (left) Clean missing dimer unit cell with random distribution of In and Ga. There is a midgap state from about 0.1 eV to 0.5 eV. On the ordered defect unit cell this state was located closer to the CB. After passivating the random defect unit cell with DMA (right) the midgap state is passivated and shifted toward the CB. Compared to the ordered DMA passivated unit cell this DOS shows a slightly narrower bandgap but the passivating effect of TMA is still evident.

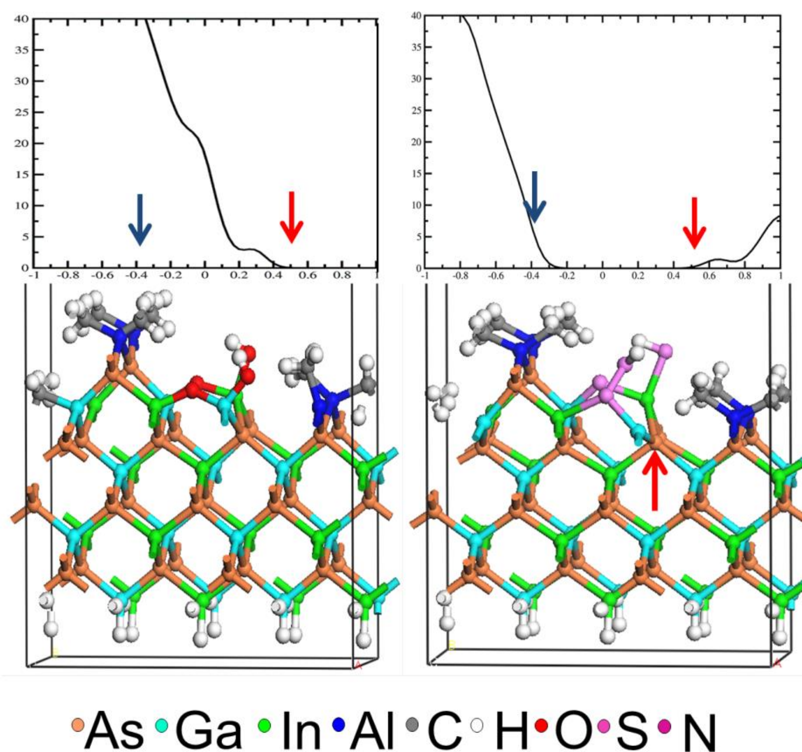

Figure 2.13. (left) DFT simulations of two O atoms inserted into the metallic bond and two –OH groups onto the edge In/Ga atoms. This system does not satisfy the electron counting rule and has excess charge resulting in a large number of valence band states. (right) DFT simulations of two S atoms inserted into the metallic bond and 2 –SH groups on the edge In/Ga atoms. One of the –SH groups migrates onto the bridging S atom. This configuration satisfies the electron counting rule and results in a clean DOS but the CB edge state is not completely suppressed due to remaining bond angle strain on the edge As atoms**.**

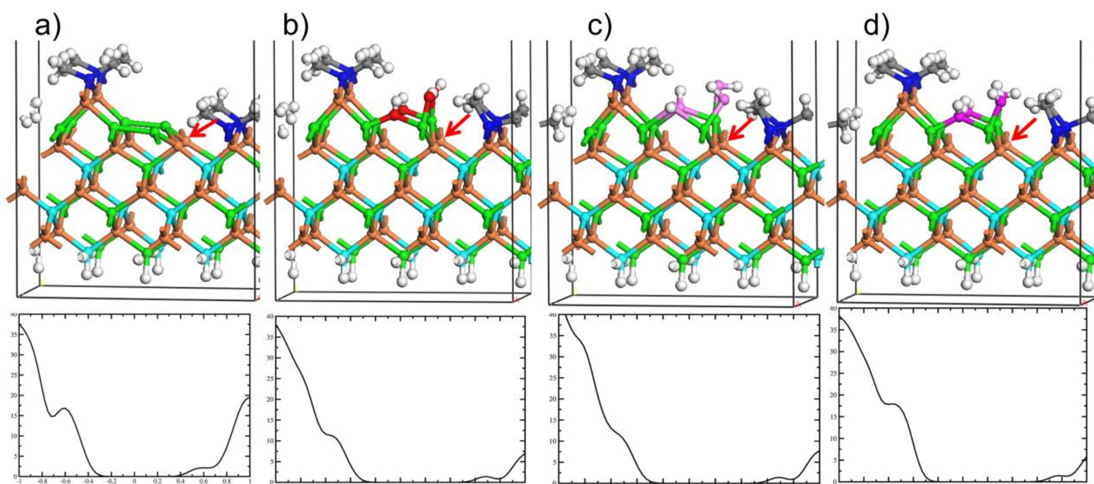

Figure 2.14. (a) TMA passivated α2 unit cell with In surface segregation. Increasing the In content of the surface shifts the onset of the CB edge state about 0.1 eV compared to the 50% In/Ga case. (b) The TMA + 4 –OH passivated case with a high In concentration shows about a 0.05 eV shift in the CB state compared to the 50% case. (c) The TMA + 4 –SH passivated case with high In concentration also has about a 0.05 eV shift in the CB state compared to the 50% case. (d) The TMA + 4 $-NH_2$ passivated case with high In concentration shows no difference in CB edge states compared to the 50% case. Surface segregation of In does not have a significant effect on this system which indicates the primary cause of the CB edge states is the As bond angle strain (red arrow) resulting from the missing As dimer that can be relieved by inserting oxidants into the metallic bonds.

2.8 References

1. H. Künzel, J. Böttcher, R. Gibis, and G. Urmann, Applied Physics Letters **61**, 1347 (1992).

2. D. M. Gill, B. Kane, S. P. Svensson, D. Tu, P. Uppal, and N. Byer, Electron Device Letters, IEEE **17**, 328 (1996).

3. W. Mönch, *Semiconductor surfaces and interfaces* (Springer, 2001).

4. S. Wilks, Journal of Physics D: Applied Physics **35**, R77 (2002).

5. H. Hasegawa, N. Negoro, S. Kasai, Y. Ishikawa, and H. Fujikuwa, Journal of Vacuum Science & Technology B **18**, 2100 (2000).

6. W. Spicer, P. Chye, C. Garner, I. Lindau, and P. Pianetta, Surface science **86**, 763 (1979).

7. P. Petroff, Journal of Vacuum Science and Technology **14**, 973 (1977).

8. P. D. Ye, Journal of Vacuum Science & Technology A: Vacuum, Surfaces, and Films **26**, 697 (2008).

9. J. Robertson, Applied Physics Letters **94**, 152104 (2009).

10. Y. Hwang, R. Engel-Herbert, and S. Stemmer, Applied Physics Letters **98**, 052911 (2011).

11. W. M. M. Edmonds, T. Kent, E. Chagarov, A. C. Kummel, ECS Transactions **50**, 129 (2012).

12. J. Shen, D. L. Winn, W. Melitz, J. B. Clemens, and A. C. Kummel, ECS Transactions **16**, 463 (2008).

13. L. Lamagna, M. Fusi, S. Spiga, M. Fanciulli, G. Brammertz, C. Merckling, M. Meuris, and A. Molle, Microelectronic Engineering **88**, 431 (2011).

14. R. Besser and C. Helms, Journal of Applied Physics **65**, 4306 (1989).

15. A. Alian, G. Brammertz, C. Merckling, A. Firrincieli, W. Wang, H. C. Lin, M. Caymax, M.Meuris, K. De Meyer, M. Heynes. Applied Physics Letters **99**, 112114 (2011).

16. V. Bessolov and M. Lebedev, Semiconductors **32**, 1141 (1998).

17. F. Capasso and G. Williams, Journal of The Electrochemical Society **129**, 821 (1982).

[18] R. Feenstra, J. A. Stroscio, J. Tersoff, and A. Fein, Physical Review Letters **58**, 1192 (1987).

[19] R. M. Feenstra, G. Meyer, F. Moresco, and K. H. Rieder, Physical Review B **66**, 165204 (2002).

[20] T. J. Kent, M. Edmonds, E. Chagarov, R. Droopad, and A. C. Kummel, The Journal of Chemical Physics **139**, 244706 (2013).

[21] C. Hinkle, A. Sonnet, E. Vogel, S. McDonnell, G. Hughes, M. Milojevic, B. Lee, F. Aguirre-Tostado, K. Choi, H. Kim. Applied Physics Letters **92**, 071901 (2008).

[22] W. Melitz, T. Kent, A. C. Kummel, R. Droopad, M. Holland, and I. Thayne, The Journal of Chemical Physics **136**, 154706 (2012).

[23] R. M. Feenstra, Surface science **299**, 965 (1994).

[24] J. A. Stroscio, R. Feenstra, D. Newns, and A. Fein, Journal of Vacuum Science & Technology A: Vacuum, Surfaces, and Films **6**, 499 (1988).

[25] G. Kresse and J. Furthmüller, Physical Review B **54**, 11169 (1996).

[26] G. Kresse and J. Furthmüller, Computational Materials Science **6**, 15 (1996).

[27] J. P. Perdew, K. Burke, and M. Ernzerhof, Physical Review Letters **77**, 3865 (1996).

[28] P. E. Blochl, Physical Review B **50**, 17953 (1994).

[29] G. Kresse and D. Joubert, Physical Review B **59**, 1758 (1999).

[30] W. Spicer, P. Chye, P. Skeath, F. C. Su, and I. Lindau, Journal of Vacuum Science and Technology **16**, 1422 (1979).

[31] W. E. Spicer, I. Lindau, P. Skeath, C. Y. Su, and P. Chye, Physical Review Letters **44**, 420 (1980).

[32] M. J. Hale, S. I. Yi, J. Z. Sexton, A. C. Kummel, and M. Passlack, The Journal of Chemical Physics **119**, 6719 (2003).

[33] H. Hasegawa and H. Ohno, Journal of Vacuum Science & Technology B **4**, 1130 (1986).

[34] P. McIntyre, Materials Research Society, Spring Meeting 2013 **CC2.06** (2013).

Chapter 3

Dual passivation of GaAs (110) surfaces using O_2/H_2O and trimethylaluminum

3.1 Abstract

The nucleation and passivation of oxide deposition was studied on defect-free GaAs (110) surfaces to understand passivation of surfaces containing only III-V heterobonds. The passivation process on GaAs (110) was studied at the atomic level using scanning tunneling microscopy while the electronic structure was determined by STS. The bonding of the oxidant and reductant were modeled with DFT. To avoid E_f pinning during gate oxide atomic layer deposition, a dual passivation procedure was required using both a reductant, TMA, and an oxidant, O_2 or H_2O. Dosing GaAs (110) with TMA resulted in the formation of an ordered complete monolayer of dimethylaluminum which passivates the group V dangling bonds but also forms metal-metal bonds with conduction band edge states. These edge states were suppressed by dosing the surface with oxidants O_2 or H_2O which selectively react with group III-aluminum bonds. The presence of an ordered Al monolayer with a high nucleation density was indirectly confirmed by XPS and STS.

3.2 Introduction

Silicon based metal oxide semiconductor field effect transistors (MOSFETs) may soon reach their physical performance limits.[1] As a consequence, many alternative semiconductors are being explored for use as channel materials. III-V semiconductors are attractive channel materials due to their high electron mobilities. A limiting factor in III-V based MOSFET performance is the high-k gate oxide/III-V interface because it usually has a large density of interfacial trap states (D_{it}).[2] Several theories have been proposed to explain the origin of interfacial trap states.[3] Studies have suggested these states are caused by native defects such as dangling bonds on the semiconductor surface, strained bonds on semiconductor surface atoms, and metal-metal bonds at the interface.[4] The majority of III-V based MOSFETs are fabricated using the group V rich (001)-(2x4) surface because this is the most easily obtained surface reconstruction.[5] This surface usually contains at least 42% defect unit cells which prevent efficient Fermi level modulation.[6] It may be possible to increase III-V based MOSFET drive current at low source-drain voltages by passivating the metallic In-Ga bonds and the strained As bonds which are present in the α2-(2x4) unit cells or by using a different crystallographic face, such as the (110) surface.

III-V (110) surfaces are an appealing alternative to traditional (001) surfaces due to their lack of group V dimers and intrinsic surface defects. III-V (110) surfaces are devoid of metallic In-Ga bonds. Instead, the surface has III-V heterobonds (i.e. no homodimers), and the surface group III-V atoms are relaxed, i.e. buckled, leaving the As atoms with filled dangling bonds in a near-tetrahedral sp^3 geometry and the group

III atoms with empty dangling bonds in a near-planar sp^2 geometry. The relaxed bonding structure results in the dangling bonds having electronic states outside of the bandgap[7] and the Fermi level of the clean surface being unpinned.

The implementation of tri-gate transistors into commercial logic chips[8] also increases the importance of III-V (110) surface passivation. The main benefits of using a fin based architecture are the reduction of short channel effects, minimized subthreshold swing, and a higher transconductance due to better electrostatic confinement.[9] The (110) surface would be the dominant surface of vertically aligned III-V (001) based finFETs[10], and with proper passivation this surface may lead to an ideal interface with the gate oxide.

In this study, the deposition of trimethylaluminum (TMA) was investigated as the Al_2O_3 seed layer on the GaAs (110) surface. While future finFETs will likely be fabricated with an InGaAs channel, GaAs was used as a model to simplify defect-free sample preparation, data interpretation, and DFT modeling. Furthermore, GaAs has a wider bandgap than InGaAs so passivation techniques developed on GaAs are likely to also be effective on InGaAs. The effects of varying the dosing and the post deposition annealing (PDA) conditions upon the formation of a highly ordered monolayer with a high nucleation density were studied since nucleation of the gate oxide atomic layer deposition (ALD) in each unit cell is critical for a minimal equivalent oxide thickness (EOT). This is the first study which uses scanning tunneling microscopy/spectroscopy (STM/STS) to study the atomic bonding configuration and electronic structure of any ALD precursor on a semiconductor (110)

surface. Since the TMA reaction on GaAs (110) results in formation of Al-Ga metallic bonds, dual passivation was investigated in which the TMA/GaAs (110) surface was dosed with H_2O or O_2. Density functional theory (DFT) calculations were performed to model the bonding configuration and density of states of the clean and TMA/oxidant deposited GaAs (110) surfaces.

3.3 Experimental

The samples were either n-type GaAs (001) wafers doped with $4x10^{18}$ cm^{-3} Si or InGaAs (110) with a dopant level of $1x10^{18}$ cm^{-3} Si on InP (110). The GaAs (001) wafers were loaded into the Omicron variable temperature UHV chamber with a base pressure of $<1x10^{-10}$ torr in a custom built cross-sectional sample holder. Samples were cleaved *in-situ* to expose the (110) crystallographic face and transferred to the scanning probe microscopy (SPM) chamber, base pressure $2x10^{-11}$ torr, where STM and STS were performed. STM was used in constant current mode to determine the atomic configuration of the surface while STS was used in variable-z mode to measure the electrical quality of the surface.[2, 11, 12] The tunneling current set point was 0.1 nA, and the samples were biased at -2.5 V. The STS curves were taken while ramping the sample bias from -2.5 V to 2.5 V and simultaneously moving the tip toward then away from the surface. All STS curves shown are an average of eight individual curves. All adsorbate structures were reproduced and the bonding configuration observed via STM and electronic structure observed via STS at least twice.

STM/STS were performed on the clean GaAs (110) surface, subsequently 10-500 Langmuirs (L) of TMA were dosed at temperatures between 25 ˚C and 200 ˚C. The samples were annealed between 135 ˚C and 350 ˚C for 30 min. All samples were annealed in ultra-high vacuum. STM was used to probe the atomic bonding structures of partial coverage and full coverage TMA surfaces. STS was used to determine Fermi level pinning of the TMA dosed surfaces. For the dual passivation studies on GaAs (110), following TMA deposition, between 1000 and 60,000 L of H_2O or O_2 were dosed at room temperature. A series of subsequent anneals were performed in 30 min increments at 250 ˚C. STM and STS were performed to observe the bonding configuration and electrical characteristics of the surface after both the TMA and the oxidant were dosed. The amounts of TMA and oxidant dosed in these experiments are generally smaller than typical ALD doses by about an order of magnitude. Auger electron spectroscopy or x-ray photoelectron spectroscopy studies were not performed on GaAs(110) since the electron/x-ray beam spot size for either instrument is larger than the exposed (110) surface.

MBE grown InGaAs (110) wafers with a dopant level of $1x10^{18}$ cm^{-3} Si on InP (110) substrate were used to determine the presence of Al on the surface with XPS. 50 L of TMA was initially dosed at 200 ˚C followed by a PDA at 230 ˚C for 30 min. Using a home-built pulsed valve system, 5 cycles of TMA/H_2O were subsequently deposited. The ALD consisted of 3 sec stabilization step for TMA, followed by a 10 sec TMA pulse/pump step in which the sample was exposed to the entire dose volume. The H_2O step was identical to the TMA step but with a 5 sec stabilization step. The

pulse lengths in this system were long due to the low vapor pressure of the precursors and the walls of the system being at 25 °C. Five additional ALD cycles were used for STS meaurments of the bandgap of the a-Al_2O_3.

An *in-situ* monochromatic XPS (XM 1000 MkII/SPHERA, Omicron Nanotechnology) was used to determine the presence of Al and O on the InGaAs (110) surface. The XPS was operated in constant analyzer energy mode with a pass energy of 50 eV and the line width of 0.1 eV using an Al Kα source (1486.7 eV). The takeoff angle was 30˚ relative the surface with an acceptance angle of 7˚. CASA XPS v.2.3 was used to analyze the data. The relative intensities of the core-level peaks were quantified by calculating the peak area and diving by the relative sensitivity factors.

All DFT simulations were performed with the Vienna Ab-Initio Simulation Package (VASP)[13, 14] using projector augmented-wave (PAW) pseudopotentials (PP)[15] and the PBE (Perdew-Burke-Ernzerhof) exchange-correlation functional.[16, 17] The choices of PBE functional and PAW PP were validated by parameterization runs demonstrating good reproducibility of experimental lattice constants, bulk moduli, and formation/cohesive energies for bulk crystalline GaAs.

3.4 Results and Discussion

3.4.1 STM of TMA deposition on GaAs (110) Surface

The cleaved GaAs (110) surface has been well studied with STM.[18-21] STM was initially employed in this study to ensure the surface was free of contaminants and

defects; Fig. 3.1(a) shows a filled state 10 x 10 nm^2 STM image of the clean GaAs (110) surface. The crystallographic directions are slightly tilted due to drift in the piezo in the scanner; this is an inherent problem which is observed in several of the images. The rows oriented in the $(\bar{1}10)$ direction are comprised of a zigzag chain of Ga and As atoms with heterobonds; this chain is depicted in a model of the clean surface shown in Fig. 3.1(b). The GaAs (110) zigzag chain is buckled so that each surface As atom is elevated relative to each surface Ga atom[22, 23] because the filled dangling bonds on the As atoms induce near tetrahedral (sp^3) bonding angles while the empty dangling bonds on the Ga atoms allow near planar (sp^2) bonding angles. The filled dangling bonds on the As atoms are directly observed in filled state STM images.

Initially, 5 L of TMA was dosed at 25 ˚C followed by an anneal at 135 ˚C for 30 min to obtain partial coverage. As shown in Fig. 3.2, STM reveals regions of the clean surface (red circle) as well as regions that have reacted with TMA (blue box). The blue box contains two sites where it is hypothesized that two TMA molecules have dissociatively chemisorbed as dimethylaluminum (DMA) between the clean GaAs rows. Line traces indicate these reacted sites are 0.5 Å above the clean surface. A reaction between TMA and the surface has occurred, but a larger dose is necessary to achieve full coverage.

Exposure of the clean surface to 10 L of TMA at 25 ˚C and a subsequent anneal at 135 ˚C for 30 min resulted in formation of ~1/3 of a monolayer (ML) of adsorbates. Ordered rows of chemisorbates formed which are rotated 40˚ clockwise

relative to the clean surface rows, as shown in Fig. 3.3. The line trace in the inset in Fig. 3.3 shows the spacing between adjacent rows was 17 Å, 3x the spacing of the clean surface rows. A proposed qualitative model for low coverage TMA chemisorption is shown in Fig. 3.3(b). Three DMA molecules reacted with the surface in a stepwise manner, giving the appearance of diagonal rows. DFT was not used to quantitatively model this system due to the size of the unit cell. For full passivation, it is necessary to increase this nucleation density while maintaining surface order.

Exposure of the clean surface to 50 L of TMA at 200 ˚C followed by an anneal at 230 ˚C for 30 min resulted in formation of an ordered monolayer of DMA with some defect sites. Fig. 3.4(a) shows the ordered rows are oriented in the $(\bar{1}10)$ direction. The spacing between adjacent rows was measured to be 5.6 Å (see insert) which is identical to the spacing of the clean surface rows indicating the maximum nucleation density has been achieved.[23] A model for the full coverage chemisorption of TMA is shown in Fig. 3.4(b). It is proposed that TMA loses a methyl group, and the resulting dimethylaluminum (DMA) makes one Al-As bond and one Al-Ga bond. This is the likely bonding geometry since bonding between adjacent As or Ga row atoms is not possible without each atom making five total bonds, which is likely energetically unfavorable. The full coverage DMA surface has three different reacted sites. The pink circle in Fig. 3.4(a) shows a dim site where DMA has bonded in the ideal configuration with rows oriented in the $(\bar{1}10)$ direction; this is the predominant chemisorption site and is modeled below with DFT to confirm the assignment. The yellow boxes show dim diagonal sites. The rows at these sites appear rotated 40˚

relative to the $(\bar{1}10)$ direction. These diagonal sites are believed to be DMA bonded between adjacent clean surface rows in a stepwise fashion giving the appearance of a diagonal row, similar to the low coverage case. The diagonal sites are never observed on the clean GaAs (110) surface. The diagonal sites are the same height as the vertical rows consistent with having nearly a full monolayer of DMA. It is noted that diagonal sites are not observed after large TMA doses (500 L). The blue triangle indicates a bright site on the full coverage surface. These are hypothesized to be AlO_x sites that form when background water in the dosing chamber reacts with the freshly deposited DMA monolayer. H_2O was not intentionally introduced into the system during this experiment. It is believed that water dissociatively chemisorbs between adjacent Al atoms and a TMA molecule subsequently chemisorbs onto the bridge bonding O atom. The height of these bright sites is 2 Å and two models have been proposed to explain these features (see below).

An annealing study was performed to determine the characteristics of DMA chemisorption on the clean GaAs (110) surface. After 500 L of TMA was dosed at 250 ˚C and subsequently annealed to 260 ˚C for 30 min, two different ordered regions appear, shown in Fig. 3.5(a). The blue arrow indicates regions of highly ordered rows with 5.6 Å spacing between adjacent rows, similar to the ideal bonding configuration in Fig. 4(a). The red arrow in Fig. 3.5(a) indicates regions with 11 Å spacing between adjacent rows, 2x the spacing of the clean surface which is not observed in the ideal TMA terminated surface shown in Fig. 3.4(a). The hemispherical bright sites (green circle), believed to be AlO_x, initially average 2.5 Å in diameter. The same sample was

subsequently annealed to 300 ˚C for an additional 60 min, shown in Fig. 3.5(b). The red box highlights regions of clean GaAs (110) that have been exposed by annealing; additionally, the AlO_x clusters have grown wider and taller with an average diameter of 3.5 Å. This suggests after annealing to 300 ˚C the bright sites (green circle) coalesce and this results in regions of TMA-free clean GaAs (110). There are also dim reacted sites (yellow triangle) that remain on the surface which are likely DMA or MMA molecules that have not desorbed. A small amount of vertical ordering remains, but the nucleation density has dramatically decreased. A final anneal to 350 ˚C for 60 min was performed, Fig. 3.5 (c), and the AlO_x clusters grew to an average diameter of 6 Å and larger regions of the clean surface became exposed, as seen in the red box in Fig. 3.5 (c). A few dim sites remain indicating sites where DMA molecules have remained in their initial chemisorption sites, but no vertical ordering is evident. There is a large thermodynamic driving force to form Al-O bonds (511 kJ/mol), and when the sample is heated, the O atoms diffuse on the surface and form highly stable clusters of AlO_x.[24] This set of experiments demonstrates that the TMA bonding is relatively weak and does not perturb the bonds within the substrate, but any oxygen present on the surface will react with Al and cluster at temperatures above 200 ˚C.

Fig. 3.6 shows an STM image obtained after dosing the full coverage DMA/GaAs (110) surface with 1000 L of O_2 at 25 ˚C followed by an anneal at 230 ˚C for 30 min and a subsequent anneal at 250 ˚C for 60 min. Ordered rows are visible in the $(\bar{1}10)$ direction (blue lines) indicating that after oxidant dosing the surface order is maintained. The dark sites (green box) are hypothesized to be sites in which a DMA

molecule has been scavenged by oxygen resulting in exposure of the clean surface while the bright sites (red arrow) are believed to be sites that have reacted with more than one –O- atom resulting in a site that is protruding from the surface, hence appearing bright in STM.

3.4.2 STS of TMA deposition on GaAs (110) Surface

STS probes the local density of states (LDOS) of the surface[11]. Experiments were only performed with n-type GaAs (110) since Fermi level pining results in a Fermi level position slightly below midgap[25] independent of n vs. p doping thereby making only measurement on n-type samples fully diagnostic.

Fig. 3.7 compares the STS spectra of the clean GaAs (110) surface and full coverage DMA surface. The clean surface (black curve) Fermi Level (E_f), which is defined as the 0 V position, is located about 0.4 V from the CB edge, consistent with an unpinned E_f.[20] The full coverage DMA surface (blue curve) shows the E_f has shifted (red arrow) and is now about 1.0 V from the CB edge, indicative of surface pinning. Additionally, a large CB edge state is observed starting at ~0.5 V. This data indicates that a highly ordered monolayer of DMA on the (110) surface pins the Fermi level near midgap consistent with DFT calculations which suggest the CB edge state is a result of Al-Ga bond formation.

STS was performed on the oxidant dosed DMA/GaAs surface. Fig. 3.8 compares the full coverage TMA surface (blue curve) with O_2 or H_2O dosed surfaces. The CB edge state is dramatically reduced after dosing the DMA surface with 1000 L

of O_2 at 25 ˚C followed by an anneal at 250 ˚C for 30 min (red curve) consistent with the hypothesis that O has inserted into the Al-Ga metallic bonds. A small CB edge states remains, indicating not all of the metallic bonds have been passivated. A subsequent 59,000 L dose of O_2 at 25 ˚C with an anneal at 250 ˚C for 30 min (olive curve) did not remove the remaining CB edge states, but it slightly shifted the E_f toward the CB consistent with further passivation. In a separate experiment, 2000 L of H_2O was dosed onto the DMA/GaAs (110) surface at 25 ˚C with a subsequent anneal at 250 ˚C for 30 min (black curve), and the CB edge states were completely passivated. It is hypothesized that the water dissociates and the –OH groups preferentially insert between the Al-Ga metallic bonds, similar to the –O- insertion, consistent with the DFT calculations below.

Since it was not possible to confirm the presence of aluminum on the cleaved GaAs (110) surface, MBE grown InGaAs (110) samples were employed to confirm a complete monolayer of DMA chemisorbs to the surface. STS was performed of the InGaAs (110) TMA/H_2O dosed surface to ensure correlation with the TMA/H_2O dosed GaAs (110) results. Fig. 3.9 compares three STS curves. The clean InGaAs (110) surface (blue) has a bandgap of about 0.8 eV. After dosing 50 L of TMA at 200 ˚C followed by an anneal at 230 ˚C for 30 min and 5 subsequent cycles of Al_2O_3 ALD (green curve) the bandgap increased to 2 eV. 30 STS spectra were taken at three different locations on the sample to ensure sample uniformity across a range of surface sites. After 10 cycles of Al_2O_3 ALD the band gap increases to 2.94 +/- 0.25 eV. The bandgap increasing to that of a thin amorphous film of Al_2O_3 after 10 cycles is

consistent with having an ordered monolayer of DMA with a high nucleation density on the InGaAs (110) surface which serves as the template for ALD of Al_2O_3.[26]

XPS was performed on the sample which had 10 ALD cycles, and it was found that the ratio of Al to O was 0.65.[24] This ideal stoichiometry also is consistent with having a very good nucleation density which allows for uniform oxide deposition.

3.4.3 Density Functional Theory Simulations

Fig. 3.10 shows a side view of DFT models and the calculated density of states (DOS) for (a) clean GaAs (110), (b) full coverage DMA, (c) –OH, and (d) –O- passivated full coverage TMA surfaces. The clean surface (a) has the buckled GaAs zigzag chains and the DOS shows a clean bandgap. This is consistent with experimental data showing the clean surface has an unpinned Fermi level. The full coverage DMA model (b) shows each Al atom bonding to an As atom and a Ga atom. The DOS shows a large conduction band (CB) edge state which is attributed to the chemisorption of TMA resulting in a metallic Al-Ga bond (red arrow). This supports the proposed model in Fig. 3.3 for DMA chemisorption in which each Al atom will make an Al-As bond and an Al-Ga bond. Experimentally, the CB edge state is observed consistent with the presence of the metal-metal bonds pinning the E_f midgap. The DFT calculated DOS shows that by inserting an –OH- group (c) into the metallic Al-Ga bond the CB edge state is fully passivated. This insertion eliminates any metallic bond character and restores the DOS to that of the clean surface. In (d), oxygen was inserted and –O- atoms bonded between the metallic Al-Ga bond and the

CB edge states were suppressed. This is a result of oxidizing the metallic bond and should result in an unpinned surface E_f. In (d), one of the methyl groups from DMA has bonded to the O atom, but the DOS shows this does not have a significant effect on the electronic structure.

Fig. 3.11 shows two different models for the bright sites observed in Fig. 3.4(a). It is proposed that in each model DMA forms a monolayer as discussed above, after formation of the initial monolayer a background H_2O or O_2 molecule dissociatively chemisorbs between (a) two DMA molecules along the GaAs (110) row direction or (b) between DMA molecules that are bonded to adjacent GaAs (110) rows. Subsequently, an additional DMA molecule from TMA was placed onto the bridging O atom since the experiments were performed with excess TMA. Note the models in Fig. 3.10 show two adjacent defect sites. The bright sites in Fig. 3.4(a) are believed to consist of only one defect site, but the double defect sites were modeled to be sure the defects do not cross react. These models result in defect sites which are about 2 Å taller than the DMA only sites. The height difference is what causes the defects to appear bright in the STM image in Fig. 3.4(a). Model (a) shows a TMA molecule as a volatile reaction product consistent with TMA having weak bonding to the bridging O atoms in part due to steric hindrance. In contrast, model (b) has C_2H_4 and H_2 as volatile reaction products consistent with DMA having ligands which readily desorb. The total energy for each system was calculated and model (a) had a total energy of -2.59 eV lower (i.e. more stable) than model (b). Since model (a) is the most thermodynamically favorable structure and it is expected that this site would

appear bright in Fig. 3.4(a) because they are about 2 Å taller than a DMA only site, this is assigned as the structure for the bright defects in Fig 3.4(a).

3.5 Conclusion

A defect-free GaAs (110) surface has been employed to nucleate the ALD of Al_2O_3 in every unit cell while maintaining a highly ordered smooth surface. Passivation of III-V (110) surfaces is especially challenging since the surfaces are dominated by heterobonds so a precursor will make bonds to both the group III and group V atoms potentially pinning the Fermi level. It was proposed that TMA dissociatively chemisorbs to the surface, making one Al-As bond and one Al-Ga bond. DFT was used to model this system and the calculated DOS show a large CB edge state which was caused by chemisorption of TMA on the surface resulting in formation of a metal-metal bond. To passivate this CB state –OH and –O- groups were inserted into the metallic bonds on the surface; in the DFT model this completely suppressed the CB edge state. Experimental work verified the theoretical work and it was shown that by starting with a clean GaAs (110) surface, it is possible to form an ordered monolayer of TMA. STS was used to verify that the TMA monolayer has a large CB edge state. By utilizing a dual passivation scheme where the TMA surface was dosed with either O_2 or H_2O this state was suppressed due to elimination of the metal-metal bonds.

3.6 Acknowledgments

Chapter 3 is in part or full, reprinted with permission from T. Kent, E. Chagarov, M. Edmonds, R. Droopad, and A. C. Kummel, "Dual passivation of GaAs (110) surfaces using O2/H2O and trimethylaluminum." The Journal of Chemical Physics **139**(24): 244706. This work was supported by the Semiconductor Research Corporation Non-Classical Research Center (SRC NCRC) task 1437.008 and by SRC Global Custom Funding.

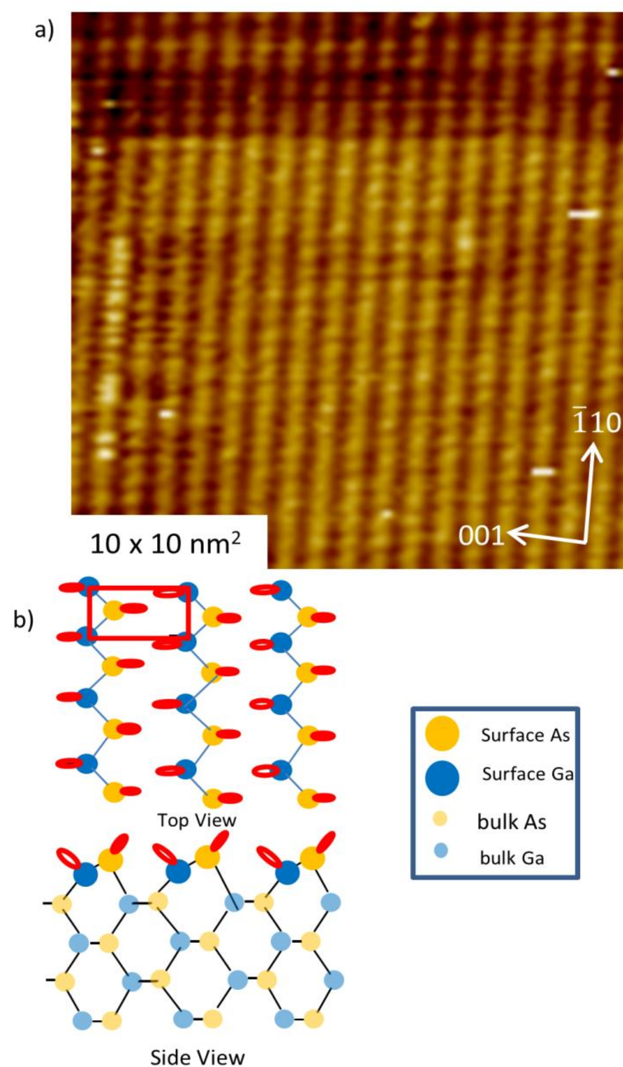

Figure 3.1. (a) A filled state STM image of the clean GaAs (110) surface. The filled dangling As bonds are directly observed resulting in rows oriented in the $\overline{(\bar{1}10)}$ direction. **(b)** A model of the clean GaAs (110) surface showing the filled As dangling bonds (filled ovals) and empty Ga dangling bonds (empty ovals) Notice the As-Ga rows are buckled which allows each As atom to be in a sp^3 geometry and each Ga to be in a sp^2 geometry

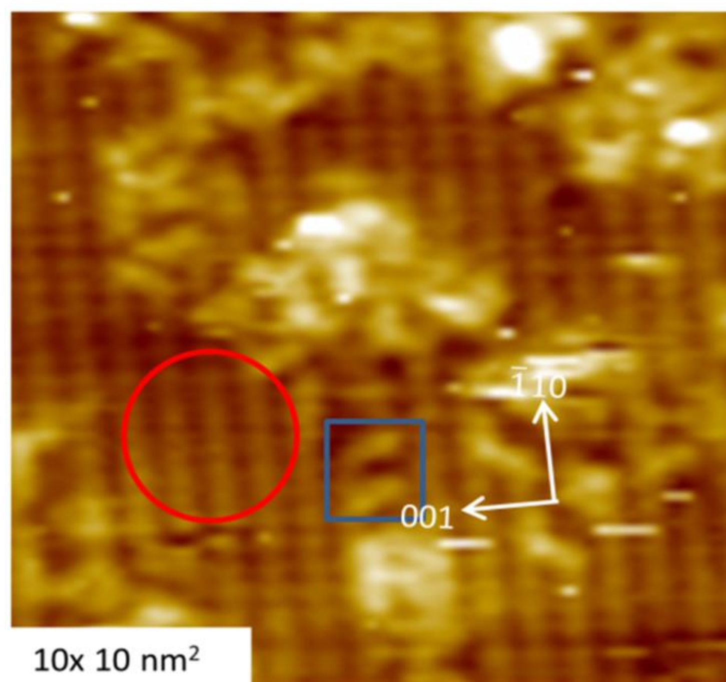

Figure 3.2. Low Coverage TMA/GaAs(110) STM image after 5 L TMA dose at 25˚C followed by a 135 ˚C anneal for 30 min. The clean surface rows are visible (red circle). Regions of TMA chemisorbates are also observed (blue box). The blue box shows two sites where DMA molecules have chemisorbed between adjacent GaAs rows. The reacted sites had a height of 0.5 Å. TMA is clearly reacting with the surface but a larger dose is necessary to obtain full coverage

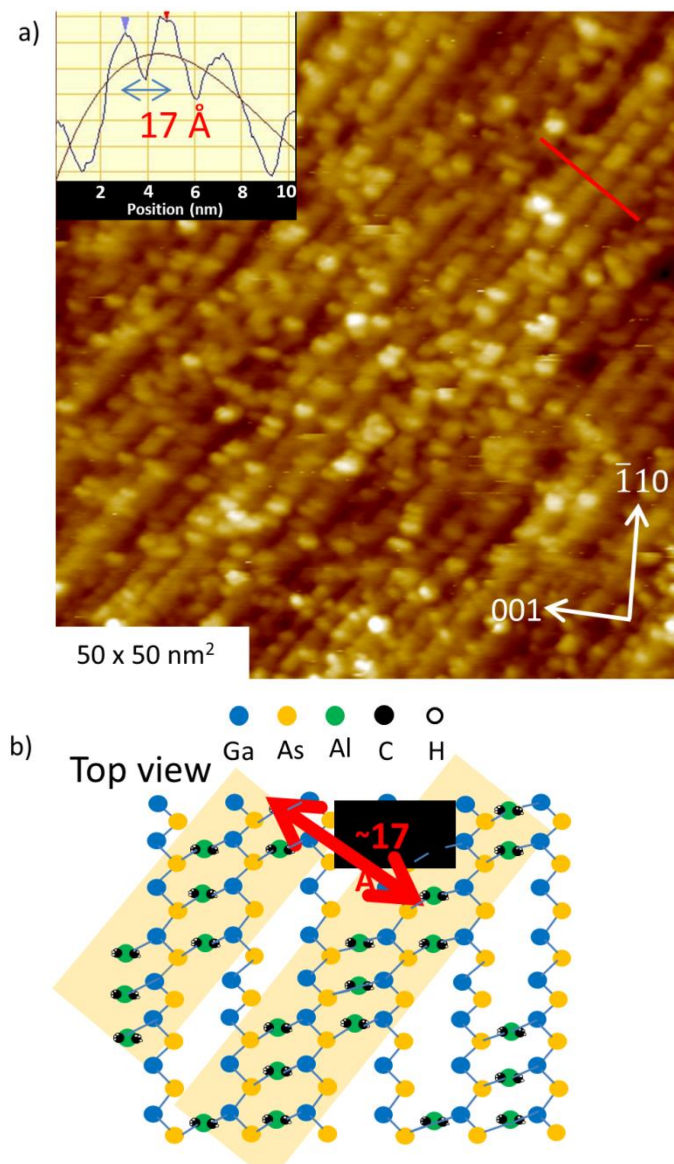

Figure 3.3. a) STM image showing 10 L dose of TMA at 25 ˚C followed by an anneal at 135˚C for 30 min. Rows are observed rotated 40˚ clockwise relative to the clean surface rows. Spacing between adjacent rows is 17 Å as shown in the line trace. b) Proposed model for low coverage TMA chemisorption on GaAs (110). TMA dissociatively chemisorbs as DMA in a stepwise fashion giving the appearance in STM of a row (orange rectangle) that is rotated 40˚ clockwise relative to the clean surface rows.

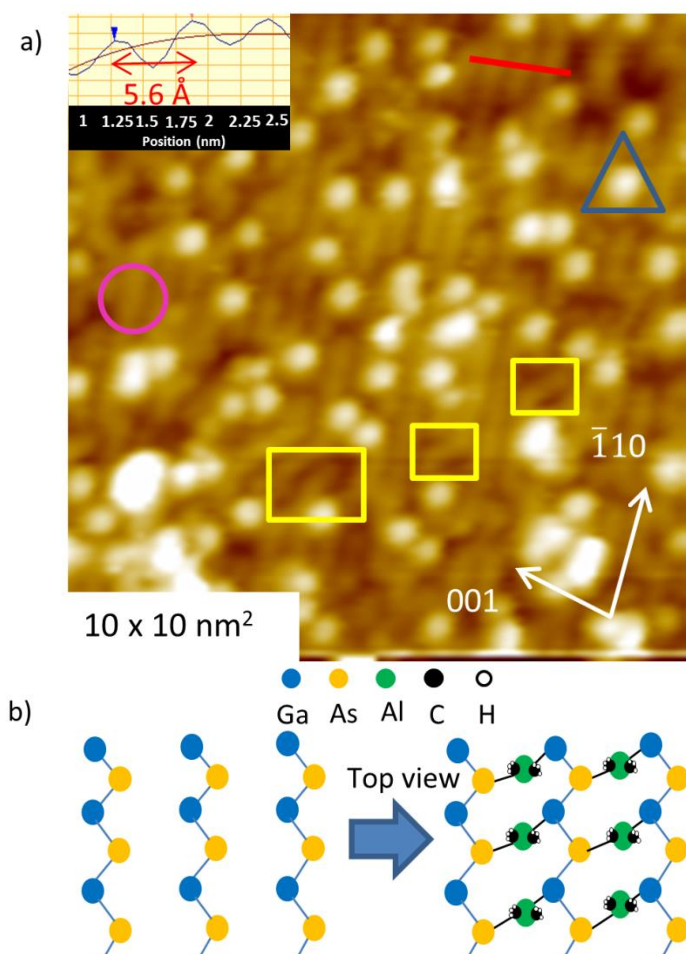

Figure 3.4. (a) An STM image of a 50 L dose of TMA at 200 ˚C followed by an anneal at 230˚C for 30 min. A complete monolayer of DMA is formed. Ordered rows of DMA (pink circle) are formed with an average of 5.6 Å between rows. This indicates the maximum nucleation density has been achieved. Diagonal sites (yellow box) are observed and are attributed to two DMA molecules chemisorbing in a stepwise fashion, similar to the low coverage case. Bright sites (blue triangle) are believed to be AlO_x. **(b)** A model for the chemisorption of TMA on the GaAs (110) surface. Each TMA loses a methyl and then bonds between adjacent GaAs clean rows forming an Al-Ga bond and a Al-As bond.

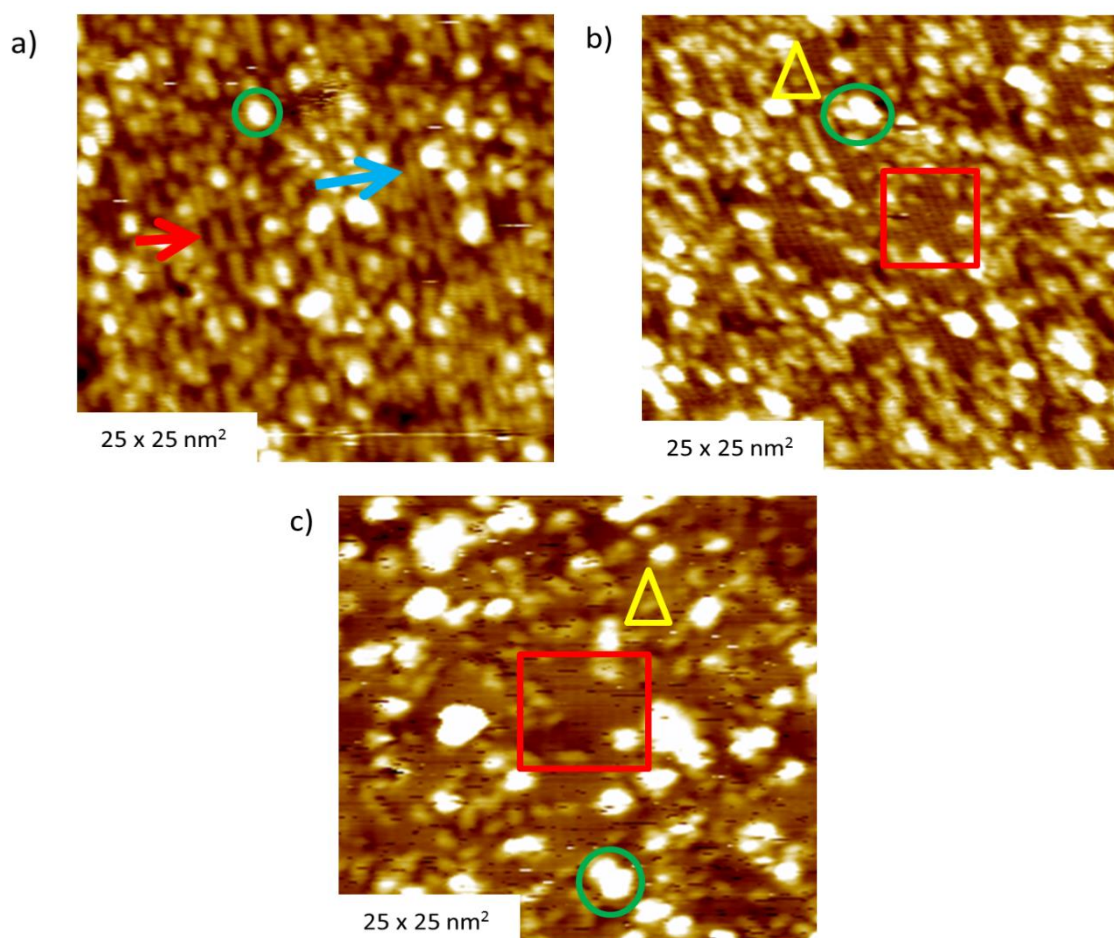

Figure 3.5. (a) STM image of 500 L TMA dose at 250 ˚C with subsequent anneal at 260˚C for 30 min. The blue arrow indicates regions with 5.6 Å spacing between adjacent rows which is observed for the full coverage surface. The red arrow indicates regions with 11 Å spacing between adjacent rows corresponding to a decreased nucleation density . There are bright sites (green circle) which are believed to be AlO_x and initially average 2.5 Å in diameter. **(b)** STM image of the same sample annealed to 300 ˚C for 60 min, areas of clean surface (red box) are visible as well as formation of large white adsorbate clusters (green circle). It is hypothesized that AlO_x clusters are coalescing which results in the larger bright sites and a larger area of exposed clean surface **(c)** Same sample annealed to 350 ˚C for 60 min. Larger areas of clean surface are visible (red box) and bright clusters continue to coalesce (green circle) with average diameters of 6 Å. DMA molecules which have remained in their initial chemisorption sites (yellow triangle) are also visible.

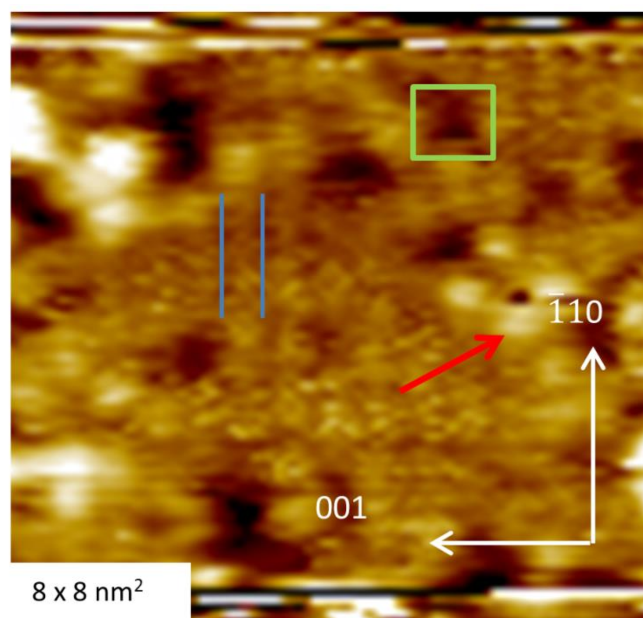

Figure 3.6. Filled state STM image of the DMA/GaAs (110) surface dosed with 1000 L of O_2 at 25 ˚C followed by an anneal at 230 ˚C for 30 min and subsequently 250 ˚C for 1 hr. Ordered rows are visible (blue lines) in the $(\bar{1}10)$ direction indicating the surface order is maintained after dosing O_2. The dark sites (green square) are hypothesized to be sites in which oxygen has scavenged a DMA molecule exposing the clean surface while the bright sites (red arrow) are hypothesized to be sites that have reacted with more than one O atom resulting in a site protruding from the surface.

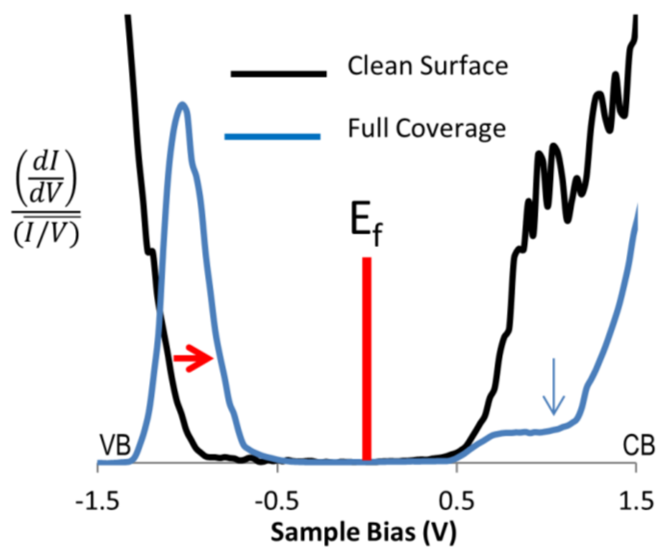

Figure 3.7. STS spectra of the clean surface (black) and full coverage TMA surface (blue). The E_f for the clean surface is located near the CB indicating an unpinned surface. The full coverage surface has a large CB edge state starting at 0.5 V and the E_f has shifted to midgap indicating the surface is pinned.

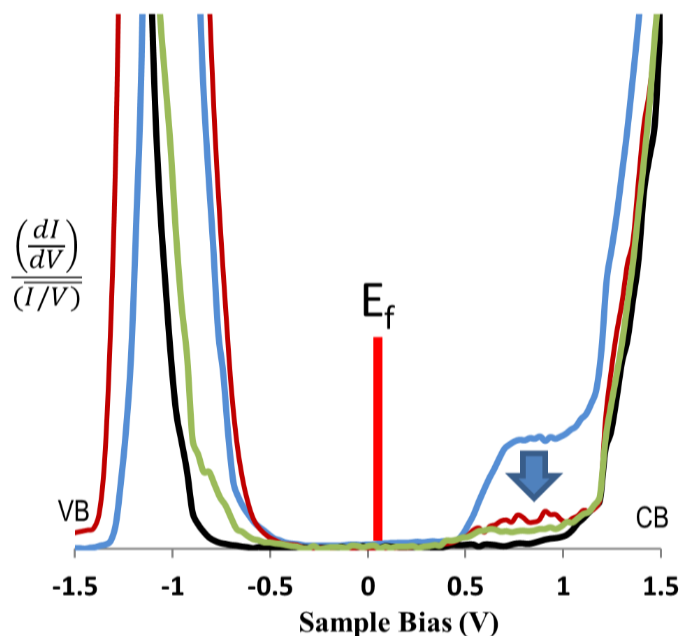

Figure 3.8. STS comparison of full coverage TMA surface (blue). Notice large CB edge state starting at 0.5 V. This sample was subsequently dosed with 1000 L O_2 at 25 ˚C and annealed to 250 ˚C for 30 min (red). The CB edge state is reduced by about 4x. The same sample was dosed with an additional 59,000 L of O_2 at 25 ˚C with an anneal at 250 ˚C for 30 min (olive). The CB edge state is further reduced but still not completely passivated. A separate experiment was performed where 2000 L of H_2O was dosed at 25 ˚C followed by an anneal at 250 ˚C for 30 min on full coverage TMA surface (black). Notice the CB edge state is completely suppressed indicating selective insertion of the oxidant into the metallic Al-Ga bonds.

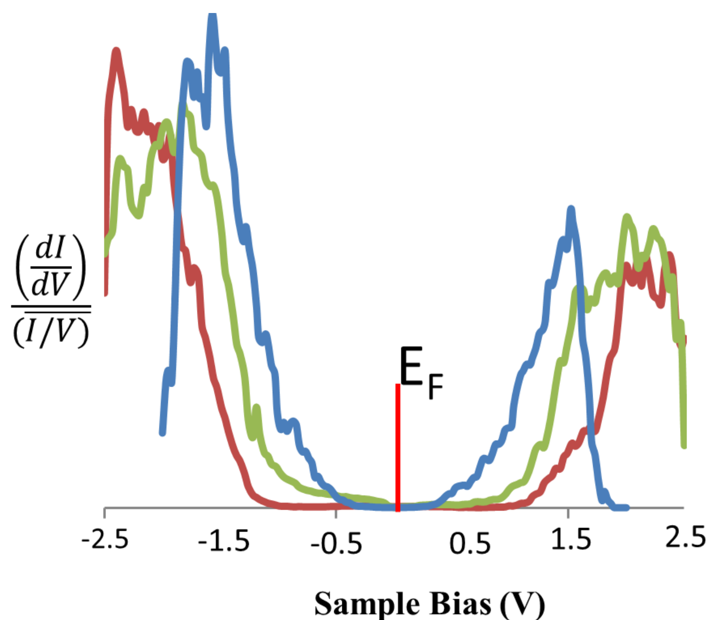

Figure 3.9. STS spectra of clean InGaAs (110) (blue) showing bandgap of 0.8 eV. Sample was subsequently dosed with 50 L of TMA at 200 ˚C and annealed at 230 ˚C for 30 min. After the initial TMA deposition Al_2O_3 was deposited in 5 ALD cycles (blue curve). The bandgap has increased to 2 eV. An additional 5 cycles of ALD were performed (red curve) and the bandgap further increased to 2.94 eV indicating a high nucleation density of the initial TMA deposition.

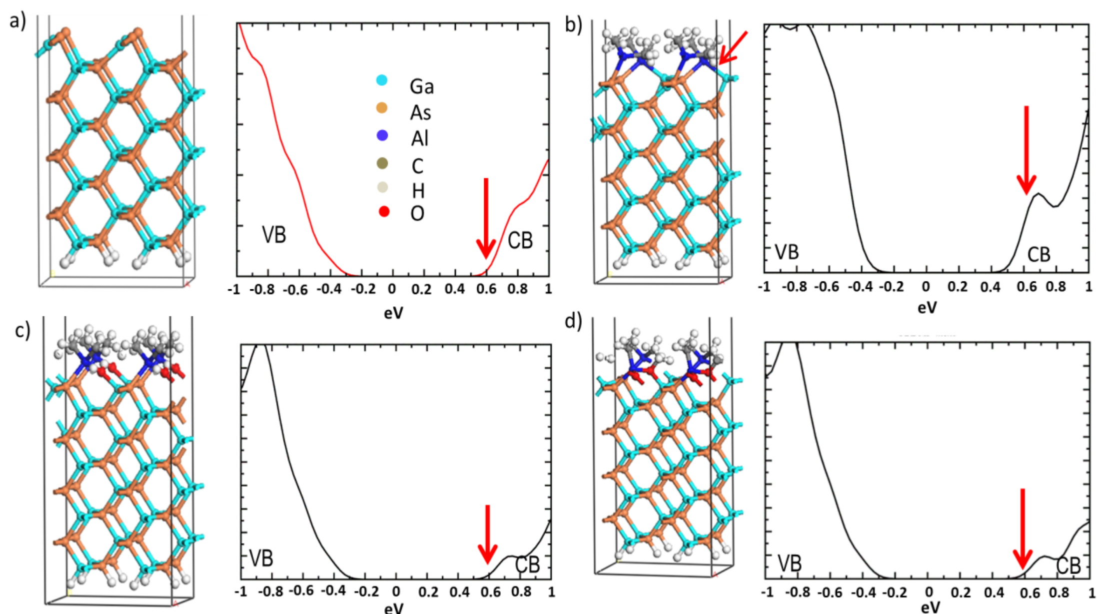

Figure 3.10. DFT model (left) and calculated DOS (right) of **(a)** clean GaAs (110) surface. The DOS shows no gap states which was experimentally verified using STS which showed the clean surface had an unpinned E_f **(b)** The full coverage DMA surface. Notice the Al-Ga bond (red arrow) which induces a CB edge state starting at 0.5 (eV). Experimentally this CB edge state is observed and pins the E_f midgap. **(c)** Model and DOS for –OH passivated DMA surface. -OH groups (red) inserted between Al-Ga bonds which eliminated the CB edge state. **(d)** Model and DOS for –O- passivated full coverage DMA surface. Notice similarities between electronic structures of c) and d).

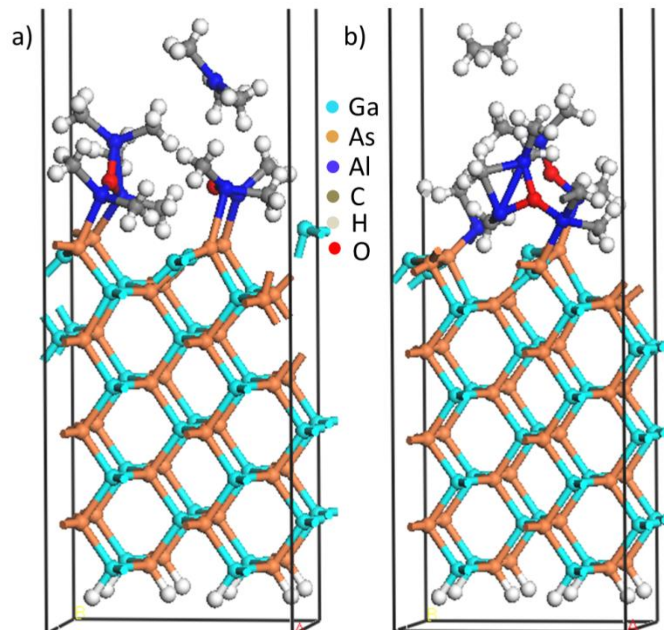

Figure 3.11. Side views of DFT models of the bright defect sites on the full coverage DMA/GaAs (110) surface. a) has an O atom bridge bonding between DMA molecules along the GaAs (110) row direction and a DMA molecule bonding on top of the O atom. This model has TMA as a volatile reaction product. (b) shows the O atom bridge bonding between DMA molecules in adjacent GaAs (110) rows with an additional DMA bonding to the O atom. This model has C_2H_4 and H_2 as volatile reaction products. Model (a) is 2.59 eV more stable than model (b).

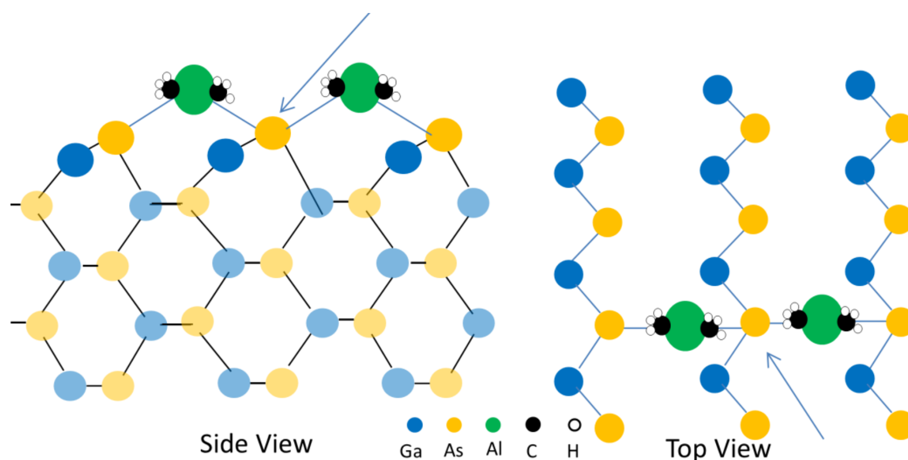

Figure 3.12. Ball and stick model of improper DMA chemisorption on GaAs (110). The arrows indicate As atoms that would make 5 bonds If each DMA molecule bonded between adjacent As atoms or adjacent Ga atoms. Each surface As or Ga is making two bonds to Al, two bonds two other surface Ga or As atoms, and one bond to a bulk As or Ga. This would likely be energetically unfavorable.

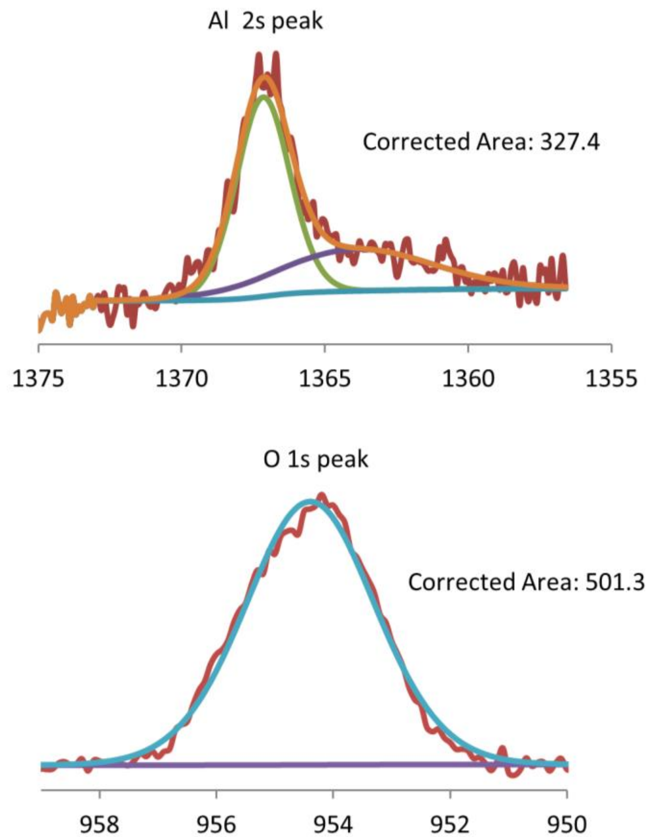

Figure 3.13. XPS peaks and corrected areas for Al 2s and O 1s after an initial 50 L TMA dose at 200 ˚C with a PDA at 230 ˚C. Subsequently 10 cycles of ALD were performed using TMA and H_2O as precursors. The Al/O ratio is 0.65. This stoichiometric oxide suggests the initial TMA monolayer had a high nucleation density and good uniformity across the sample.

3.7 References

[1] M. M. Heyns, Solid State Phenomena **187**, 3 (2012).

[2] W. Mönch, *Semiconductor surfaces and interfaces* (Springer, 2001).

[3] P. D. Ye, Journal of Vacuum Science & Technology A: Vacuum, Surfaces, and Films **26**, 697 (2008).

[4] J. Robertson, Applied Physics Letters **94**, 152104 (2009).

[5] Y. Hwang, R. Engel-Herbert, and S. Stemmer, Applied Physics Letters **98**, 052911 (2011).

[6] W. M. M. Edmonds, T. Kent, E. Chagarov, A. C. Kummel, ECS Transactions **50**, 129 (2012).

[7] W. E. Spicer, I. Lindau, P. Skeath, C. Y. Su, and P. Chye, Physical Review Letters **44**, 420 (1980).

[8] C. Auth, C. Allen, A. Blattner, D. Bergstrom, M. Brazier, M. Bost, M. Buehler, V. Chikarmane, T. Ghani, T. Glassman. *VLSI Technology (VLSIT), 2012 Symposium on* (IEEE, 2012), p. 131.

[9] D. Hisamoto, T. Kaga, Y. Kawamoto, and E. Takeda, in *Electron Devices Meeting, 1989. IEDM'89. Technical Digest., International* (IEEE, 1989), p. 833.

[10] M. Jurczak, N. Collaert, A. Veloso, T. Hoffmann, and S. Biesemans, in *SOI Conference, 2009 IEEE International* (IEEE, 2009), p. 1.

[11] R. M. Feenstra, Surface science **299**, 965 (1994).

[12] J. A. Stroscio, R. Feenstra, D. Newns, and A. Fein, Journal of Vacuum Science & Technology A: Vacuum, Surfaces, and Films **6**, 499 (1988).

[13] G. Kresse and J. Furthmuller, Computational Materials Science **6**, 15 (1996).

[14] G. Kresse and J. Furthmuller, Physical Review B **54**, 11169 (1996).

[15] J. P. Perdew, K. Burke, and M. Ernzerhof, Physical Review Letters **77**, 3865 (1996).

[16] P. E. Blochl, Physical Review B **50**, 17953 (1994).

[17] G. Kresse and D. Joubert, Physical Review B **59**, 1758 (1999).

[18] J. Zheng, X. Liu, N. Newman, E. Weber, D. Ogletree, and M. Salmeron, Physical Review Letters **72**, 1490 (1994).

[19] G. Lengel, R. Wilkins, G. Brown, and M. Weimer, Journal of Vacuum Science & Technology B: Microelectronics and Nanometer Structures **11**, 1472 (1993).

[20] R. M. Feenstra, G. Meyer, F. Moresco, and K. H. Rieder, Physical Review B **66**, 165204 (2002).

[21] R. Feenstra, J. A. Stroscio, J. Tersoff, and A. Fein, Physical Review Letters **58**, 1192 (1987).

[22] G.-X. Qian, R. M. Martin, and D. J. Chadi, Physical Review B **37**, 1303 (1988).

[23] J. L. A. Alves, J. Hebenstreit, and M. Scheffler, Physical Review B **44**, 6188 (1991).

[24] J. Kerr, CRC Handbook of Chemistry and Physics, 81st ed., CRC Press, Boca Raton, FL, USA (2000).

[25] K. Stiles and A. Kahn, Physical Review Letters **60**, 440 (1988).

[26] V. Rose and R. Franchy, Journal of Applied Physics **105**, 07C902 (2009).

Chapter 4

The Influence of wet and dry native oxide removal on the nucleation of low temperature HfO_2 ALD on InGaAs (001) and (110) surfaces

4.1 Abstract

Current logic devices rely on 3D architectures, such as the finFET, which utilize the (001) and (110) crystal faces simultaneously thus requiring passivation methods for the (110) face in order to ensure a pristine 3D surface prior to further processing. An additional challenge for III-V semiconductor based FETs is the large density of trap states at the semiconductor/oxide interface. Several surface cleaning and passivation techniques were examined with the goal of maximizing the nucleation density of HfO_2 on both the InGaAs (001) and (110) surfaces. STM and XPS were utilized to compare and contrast the effects of a previously developed in-situ pre-ALD surface clean on the InGaAs (001) and (110) surfaces. MOSCAPs were fabricated in order to compare electrical results with observations made with STM and XPS. *Ex situ* wet cleans are very effective on the (001) surface but not the (110) surface. CV indicated the (001) surface with no BOE had a higher C_{max} hypothesized to be a result of poor nucleation of HfO_2 on the native oxide. An *in situ* pre-ALD surface clean employing both atomic H and TMA pre-pulsing, developed by Chobpattana et al. and Carter et al. for the (001) surface, was demonstrated to be effective on the (110) surface for producing low D_{it} high C_{ox} MOSCAPs. Including TMA in the pre-ALD surface clean resulted in reduction of the magnitude of the interface state capacitance.

The XPS studies show the role of atomic H pre-pulsing is to remove both carbon and oxygen while STM shows the role of TMA pre-pulsing is to eliminate H induced etching. Devices fabricated at 120 ˚C and 300 ˚C were compared.

4.2 Introduction

A major obstacle facing III-V based transistors is the increased power dissipation that results from subthreshold leakage current, band to band tunneling, and aggressive gate oxide scaling.[60, 61] Tunneling through the gate oxide exhibits an exponential dependence on oxide thickness, and scaling dielectric below 1 nm equivalent oxide thickness (EOT) results in unacceptable leakage currents.[62, 63] In order to minimize gate leakage, without sacrificing capacitance, high-k materials can be employed. This allows for a physically thicker oxide and equal or higher capacitances than for traditional SiO_2 dielectrics.[64] Utilizing high-k materials such as HfO_2 and Al_2O_3 has already allowed for EOT below 1 nm and devices that outperform traditional Si based metal oxide semiconductor field effect transistors (MOSFETs).[65, 66] To continue aggressively scaling the gate oxide it is crucial to maximize the nucleation density of the high-k atomic layer deposition (ALD) precursors, so that the dielectric closes to form a continuous film on the substrate in a small number of ALD reaction cycles.

Compound semiconductor based MOS devices also suffer from a relatively high density of interface trap states (D_{it}) at the semiconductor/high-k interface. These electronic trap states result from physical defects at the interface such as dangling

bonds, metallic bonds, strained bonds, and defective native oxides. These can result directly from poor initiation of high-k ALD on the semiconductor surface.[3, 4, 8] To increase drive current and minimize power consumption of III-V devices, it is important to minimize the D_{it}. Subcutaneous oxidation of the substrate and plasma induced damage during pre-ALD surface cleans can also generate D_{it}. It is possible to utilize hydrogen to remove native oxide as demonstrated by Melitz et. al.[67] Carter et al. and Chobpattana et al. demonstrated that by utilizing TMA and H_2 plasma prior to ALD of Al_2O_3 and HfO_2 capacitance voltage (CV) characteristics can be improved at 300 ˚C.[68, 69]

In this study, a pre-ALD *ex situ* wet clean and *in situ* dry etch were examined on both InGaAs (001) and InGaAs (110) surfaces in order to determine their effects on the nucleation of HfO_2 during ALD at 120 ˚C. In the absence of TMA in the process, low ALD temperature is of interest in order to minimize hydrogen plasma damage of both the (001) and (110) surfaces and to limit subcutaneous oxidation of the substrate by H_2O and O_2, both of which can diffuse through HfO_2.[70] Scanning tunneling microscopy was used to gain an atomic level understanding of the processes occurring during the *in situ* clean. X-ray photoelectron spectroscopy (XPS) and CV analysis were used to determine the effect of a buffered oxide etch (BOE) on the nucleation of HfO_2.

4.3 Experimental

MOSCAPs were fabricated with 300 nm of InGaAs (001) grown by molecular beam epitaxy (MBE) with 1x10^{17} cm^{-3} Si doping on n-type InP (001) substrates. The InGaAs (110) samples were grown by MBE with 1x10^{17} cm^{-3} Si doping on InP (110) substrates. MOSCAP samples were initially degreased for 3 min in acetone, isopropyl alcohol (IPA), and deionized (DI) water. Immediately prior to loading samples into the ALD chamber, for some samples, the native oxide was removed with a 3 min dip in a BOE solution comprised of a 30:4 ratio of 36% NH_4F and 8% HF followed by a 1 min rinse in DI water. Samples were quickly loaded (1-2 min air exposure) into an Oxford Instruments FlexAL ALD reactor. Some samples received an *in situ* surface clean prior to ALD consisting of a 20 mTorr inductively coupled 100 W H_2 plasma for 2 sec, 40 ms of 200 mTorr TMA, and another H_2 plasma pulse. For some experiments, the TMA pulse was eliminated.[68, 69] For samples deposited with HfO_2 at 120 ˚C, an ALD cycle consisted of a 1 sec pulse of 80 mTorr tetrakis(ethylmethylamino)hafnium (TEMAH), a 7 sec Ar purge, a 1 sec 80 mTorr H_2O pulse, and a 35 sec purge. For samples deposited with HfO_2 at 300 ˚C a 1 sec 80 mTorr pulse of TEMAH, 5 sec Ar purge, 5 sec pump, 0.05 sec 80 mTorr H_2O pulse 7 sec Ar purge, 7 sec pump, were employed. All samples underwent a 15 min 400 ˚C forming gas anneal (FGA, 5% H_2, 95% N_2) prior to metal deposition. The gate metal was 50 nm thick thermally evaporated Ni deposited in 150 μm diameter circular electrodes using a shadow mask. The backside contact was a blanket deposited 20 nm thick thermally evaporated Ni film coated by 80 nm of thermally evaporated Au. CV, IV curves were measured

using a HP4284A LCR meter and an Agilent B1500 Semiconductor Device Analyzer. The frequency range of all CV measurements is from 1 kHz (blue) to 1 MHz (grey). All D_{it} values were calculated using the full interface state model.[71] At least 10 CV measurements were performed on separate gates for each sample to ensure uniformity across the sample.

InGaAs (001) samples used for STM were grown by MBE with $1x10^{18}$ cm^{-3} Si doping on InP (001) substrates and were capped with 50 nm of As_2. Samples were loaded into a variable temperature Omicron ultrahigh vacuum chamber and the As_2 cap was removed by heating the samples to 350 ˚C for 30 min and the (2x4) reconstruction was obtained by heating to 400 ˚C for at least 30 min. Details of the (2x4) reconstruction are given elsewhere.[26, 35] Samples were subsequently exposed to atomic H generated from an Oxford Applied Research TC-50 thermal gas cracker. The hydrogen doses are reported in Langmuir (1 L = 1 sec at 1x 10^{-6} torr) based on the H_2 pressure; however, the cracking efficiency is reportedly to be closer to 50% (Oxford Applied Research) but could not be verified; therefore the reported atomic H doses are an upper limit. Various amounts of TMA were also deposited on the samples; details of specific dose amounts of atomic H and TMA are given in the results section. After dosing, samples were transferred to the scanning probe microscopy (SPM) chamber, base pressure ~$1x10^{-11}$ torr. Scanning tunneling microscopy (STM) was performed using a tunneling current set point of 100 pA and a constant tip-sample bias of -3.0 V. All STM images were reproduced at least twice. XPS was performed with a monochromatic XM 1000 MkII/Sphera system developed

by Omicron Nanotechnology. A constant analyzer pass energy of 50 eV was employed with a 0.1 eV linewidth obtained using a monochromatic Al Kα source (1486.7 eV). The takeoff angle was 30 ˚ relative to the surface (surface sensitive) with an acceptance angle of 7 ˚. All spectra were analyzed with CASA XPS v. 2.3.

4.4 Results and Discussion

4.4.1 In-situ native oxide/contaminant removal

The effect of TMA incorporation into the *in situ* pre-ALD surface clean was investigated by fabricating MOSCAPs on InGaAs (001) with 10 cycles of either H plasma alone or H/TMA/H followed by 40 cycles of HfO_2 ALD at 120 ˚C or 300 ˚C. The sample in Fig. 1 (a) received 10 cycles of H plasma at 300 ˚C while Fig. 1(b) had 10 cycles of H/TMA/H at 300 ˚C. It is evident that the H plasma damaged the InGaAs surface, resulting in both a large false inversion bump (at negative gate bias), which is attributed to interface trap states,[5, 6] and the dispersion in the depletion regime (gate bias ~ +0.5 V). After incorporation of TMA into the pre-ALD clean the peak value of the interface state capacitance was reduced from 1.88 $\mu F/cm^2$ to 0.5 $\mu F/cm^2$ at 1 kHz, and the dispersion in depletion was reduced. This indicates that TMA exposure minimized the plasma induced damage to the surface resulting in a significant reduction in interfacial trap density. The same experiment was performed at 120 ˚C and the amount of plasma damage was reduced by temperature alone, Fig. 1(c), without adding TMA to the pre-ALD plasma treatment. The peak capacitance of the

false inversion bump at 1 kHz for the 120 ˚C case was 0.93 μF/cm^2 compared to 1.88 μF/cm^2 for the 300 ˚C case, but dispersion throughout the depletion region remains. After incorporating TMA at 120 ˚C, the 1 kHz peak value of the interface state capacitance was further reduced to 0.59 μF/cm^2 and the dispersion in the flatband region was reduced; as shown below this corresponds to approximately 25% decrease in the peak D_{it} near the CB. It has been shown previously that utilizing atomic H, TMA, and TEMAH can remove native oxides on III-V surfaces[34, 67], but this result indicates the TMA is playing an additional role in minimizing defect formation at both high and low temperatures.

STM was employed to determine the passivating mechanism of TMA in the pre-ALD surface clean. Previous work by Melitz et al. utilized STM to show that atomic H removes carbon and oxygen from the surface but produces a high density of etching pits; here the co-dosing of H and TMA was investigated to understand how the TMA prevents atomic H induced etching damage.[67] Fig. 2(a) shows a 50 x 50 nm^2 STM image of the clean InGaAs (2x4) surface. Details of the clean (2x4) surface have been discussed in detail elsewhere.[26] After exposing the clean surface to 1800 Langmuir (L) of atomic H at 300 ˚C, bright sites with an average width and height of 5.79 nm and 0.4 nm are observed, Fig. 2(b). Atomic H is known to etch III-V surfaces; after native oxide removal, AsH_3 is the first species to thermally desorb.[72] Previous studies have indicated Ga droplet formation can occur due to an increase in the Ga mobility as arsenic hydride species desorb.[73, 74] It is hypothesized the clusters observed are metallic In/Ga clusters. Metallic bonds are known to induce trap states at

semiconductor oxide interfaces consistent with the large false inversion bump observed in Fig. 1(a).[75, 76]

Fig. 2(c) shows the surface after an initial 10,000 L dose of TMA at 300 ˚C followed by a subsequent 1800 L dose of atomic H at 300 ˚C. The height, width, and density of the bright sites have been reduced but not eliminated. It is hypothesized that after monolayer deposition of TMA, the atomic H reacts with the dissociated methyl groups forming methane which desorbs. XPS below shows not all of the $-CH_3$ groups are removed; the surface is covered with $Al(CH_3)_x$ groups which protect it from etching by blocking reaction between additional atomic H and substrate As, consistent with previous studies showing that the $Al(CH_3)_x$ bonds to the As atoms.[77]

To determine if TMA could further reduce atomic H induced etching defects, the clean surface was dosed with TMA, then atomic H, and a final dose of TMA, Fig. 2(d). Afterwards, the surface shows almost complete elimination of bright clusters; the surface is atomically ordered with 1.7 nm between adjacent rows (inset), and atomically flat indicated by presence of a single atomic step. This implies TMA not only prevents plasma damage but also cleans up any residual damage. A possible mechanism is the incoming TMA reacts with the In/Ga clusters, forming trimethylgallium (TMG) or trimethylindium which desorb. The vapor pressure of TMG at 25 ˚C is 226.58 torr while the vapor pressure of TMA is 11.38 torr suggesting desorption of TMG is likely.

The number of pre-ALD cycles was optimized to ensure effective removal of native oxide and surface contaminants to maximize the nucleation density of HfO_2

while minimizing plasma induced damage. Fig. 3 (top) shows InGaAs (001) samples which have received 2, 5, and 10 cycles of the H/TMA/H pre-ALD clean followed by 30 cycles of HfO_2 ALD at 300 ˚C. Utilizing 2 cycles of the pre-clean resulted in a C_{max} at 1 kHz of 2.75 $\mu m/cm^2$ which was reduced to 2.4 $\mu F/cm^2$ when employing 5 or more cycles. This suggests that the nucleation density of HfO_2 after 2 cycles is lower than when using 5 cycles due to native oxide and/or contaminants remaining on the surface. The reduction in C_{max} is attributed to more efficient cleaning of the surface with increased H Plasma cycles rather than AlO_x deposition from background water reacting with TMA. This results in a thinner overall oxide and, therefore, a slightly higher $C_{max.}$ The dispersion in accumulation and the flatband regions remain similar for all cases while the false inversion bump is slightly reduced as the number of cycles increase. The weak inversion frequency response of MOS capacitors is increasingly sensitive to D_{it} as the C_{max} value, indicative of the oxide capacitance, decreases.[78] Therefore, the smaller interface trap humps in the inversion region seen in Fig. 3 for increasing numbers of H/TMA/H cleaning cycles is consistent with removal of defect-inducing adsorbates on the InGaAs surface that create interfacial trap states. Additionally, despite a 5x increase in H plasma exposure, no damage is evident in the CV profile, emphasizing the protective role of TMA in the pre-ALD clean.

Performing the same experiments at 120 ˚C, Fig. 3 (bottom), indicates that, at lower temperatures, at least 10 H/TMA/H cycles are required to maximize the effectiveness of the plasma treatment and enhance the nucleation of HfO_2 during subsequent ALD. The C_{max} value continually decreases as the number of pre-ALD

cycles increases, suggesting it is more difficult to remove oxide or contamination at low temperatures. The frequency dispersion of capacitance in accumulation and depletion show no significant change among the samples, but D_{it} hump in the inversion region does decrease with increasing number of cycles, as for the 300 ˚C ALD condition. Again, despite a 5x increase in plasma exposure, we see no evidence of plasma damage, highlighting the importance of TMA in this process. When 20 cycles are employed there is noticeable plasma damage (not shown).

4.4.2 Ex-situ native oxide removal

Wet BOEs are routinely used to remove oxide from III-V substrates prior to processing. The effect of the BOE on both (001) and (110) surfaces and its impact on HfO_2 nucleation at 120 ˚C and 300 ˚C was studied. Fig. 4 compares (001) and (110) samples which received a BOE (left column) and did not receive a BOE (right column) at 120 ˚C. The wet cleaned samples were loaded into the ALD reactor with a maximum 2 min air exposure. All four samples were in the ALD reactor simultaneously to ensure identical deposition conditions, and each received 10 cycles of H/TMA/H pre-ALD surface clean and 30 cycles of HfO_2 ALD. The (001) sample which received the BOE shows a maximum capacitance at high frequency of ~2 $\mu F/cm^2$ whereas the sample which did not receive the BOE shows a C_{max} of ~2.6 $\mu F/cm^2$. It is hypothesized that the native oxide on the non-BOE sample limits the nucleation of HfO_2 on the (001) surface. Limited nucleation would result in a thinner overall oxide and, therefore, a higher C_{max}. Additionally, the non-BOE sample shows

a slightly D_{it} hump in the inversion region. This can be attributed to the presence of a variety of InGaAs native oxides which are known to be a source of trap states in III-V based devices.[3, 79, 80] The (110) surface shows no significant difference between the wet cleaned and non-wet cleaned samples. This indicates HfO_2 is nucleating identically on both samples suggesting the BOE is not effective on this surface or that the (110) surface has such a thin native oxide that the BOE etch is immaterial when *in situ* atomic H is employed, consistent with the XPS data described later in this report.

The same experiment was performed at 300 ˚C except the samples received 48 cycles of HfO_2 ALD to account for a lower growth rate, Fig. 5. Similar behavior was observed for the (001) InGaAs samples. The C_{max} for the non-BOE sample was 2.8 μF/cm^2 compared to ~2.4 μF/cm^2 for the sample which received a BOE. It is hypothesized that the HfO_2 is not nucleating as efficiently on the sample with a thicker native oxide, resulting in a thinner HfO_2 layer. The interface trap responses in the inversion region of the associated MOSCAPs are comparable, which can be attributed to the increased effectiveness of the H plasma at 300 ˚C. For the (110) samples, the C_{max} of the sample which did not receive a BOE is within 10% of the C_{max} of the BOE sample and thus not material. The leakage current densities of the 300 ˚C samples were much higher than the 120 ˚C samples, Fig. 4.6. For example the 120 ˚C InGaAs (001) and InGaAs (110) samples had about 100x lower leakage current density at +1 V relative to the flatband voltage (V_{fb}) than the corresponding 300 ˚C samples. This may be due to the presence of a small CVD component in the 120 ˚C ALD recipe which resulted in thicker oxides. At 120 ˚C the growth rate per cycles was ~1.4

Å/cycle while at 300 ˚C the growth rate was closer to 1Å/cycles as measured by ellipsometry.

X-ray photoelectron spectroscopy (XPS) was used to investigate the composition of the (001) and (110) surfaces after the BOE and during the H/TMA/H pre-ALD clean. The integrated carbon and oxygen 1s signals are normalized to the sum of the In 3d, Ga 2p, and As 3d peaks in the bar chart in Fig. 6. The red column is the initial sample, green is after the first atomic H dose, purple after a subsequent TMA dose, and blue after the final atomic H clean. The same process matrix is presented as in Figs. 4 and 5. The H/TMA/H dosing was performed at 120 ˚C. The as-loaded (001) samples which did not receive a BOE exhibit much higher levels of carbon and oxygen than the (001) BOE sample, which is expected. The initial (110) sample which received a BOE shows a reduction in carbon compared to the non-BOE sample, but the oxygen surface composition of both the non-BOE and BOE samples are almost identical. The (110) surface is inherently more stable than the (001) surface and may be less prone to oxidation than the (001) surface due to its simple surface reconstruction.[55, 81] The ineffectiveness of the BOE to remove the oxygen on the (110) surface mirrors the similar CV curves observed in Fig. 4. After exposing both (001) samples to 1800 L of atomic H at 120 ˚C (green bars), the amount of C and O are reduced to similar levels on both non-BOE and BOE samples. The (110) surface exhibited the same trend and the atomic H reduced the ratio of carbon to InGaAs to about 0.2-0.3 while the ratio of oxygen to InGaAs was reduced to less than 0.1. It was not expected that the atomic H would remove all the surface carbon in a single dose

because the cyclic H/TMA process is designed to concurrently remove carbon bonded to InGaAs while protecting the surface dosed with TMA which has carbon bonded to Al.

As shown in purple bars in Fig. 6, all samples show an increase in carbon after a subsequent 10,000 L dose of TMA due to the deposition of methyl groups. The blue bars in Fig. 6 show a final dose of atomic H results in reduction of carbon signal due to desorption of methane and/or removal or additional surface carbon and the oxygen signal remains just above the detection limit of the XPS. This study emphasizes the need for an in-situ dry surface cleaning method. The ex-situ BOE did not have the same cleaning effects on both the (001) and (110) surface while the atomic H had a very similar cleaning effect on both surfaces. In fabricating a 3D device, it is crucial to simultaneously clean all faces of the devices to ensure pristine surfaces prior to further processing.

The D_{it} energy profiles of several of the samples from Figs. 1-5 were extracted using the full interface state model, Fig. 7.[71] The sample which was exposed to 10 cycles of H plasma at 300 ˚C (red square) exhibits a dramatically higher D_{it} than any of the other samples, which was suggested by the magnitude of the false inversion bump. The sample that was exposed to atomic H at 120 ˚C (purple x) exhibits a slightly higher D_{it} than any of the other samples in the upper half of the bandgap. All samples which had TMA incorporated into the pre-ALD clean, regardless of the process temperature or *ex situ* BOE cleaning, exhibit very similar D_{it} values of 2 - 3.8 x 10^{12} cm^{-2} eV^{-1} at $E-E_c = -0.5$, Table 1. The samples do show a greater variation in

the D_{it} toward the VB. However, in an n-channel flat band architecture III-V MOSFET, the Fermi level is only modulated in the upper half of the band gap making interface states below the mid gap less significant for limiting device performance. A method for extracting the border trap densities (N_{bt}) was developed by Taur et al. which assumes a spatially uniform N_{bt} distribution in the oxide and takes into account the influence of C_{max} on frequency dispersion in accumulation. The densities are extracted by matching the frequency dispersion at the accumulation regions of both the CV and GV curves.[82] The border trap densities (N_{bt}) were also extracted, Table 1. All samples which had TMA incorporated into the pre-ALD surface clean had N_{bt} values between 1.7 and 2.4 x 10^{20} cm^{-3} eV^{-1}. The sample which was exposed to H only at 300 ˚C had an N_{bt} of 3.0 x 10^{20} $cm^{-3}eV^{-1}$. The majority of samples processed at 120 ˚C had a lower D_{it} than the samples processed at 300 ˚C and statistical analysis showed, using an alpha value of 0.05, a p value of < 0.05 indicating lowering the ALD temperature resulted in reduction of D_{it}. An α value of 0.05 indicates the results have 95% chance of being due to manipulation of experimental variables while obtaining a p value less than the α value, (< 0.05), suggests that these results are due to the temperature differences. This indicates TMA-based surface treatment not only reduces the density of defects at the InGaAs/HfO_2 interface but also results in a more robust oxide, as border traps are associated with defects within the oxide and are thought to be located within about 1 nm from the semiconductor/oxide interface.[15]

4.5 Conclusion

In situ STM/STS and XPS were employed to determine the role of TMA in a pre-ALD surface clean developed by Carter et al. and Chobpattana et al. and to determine the effectiveness of this clean on the InGaAs (110) surface. By employing STM, XPS, and CV profiling TMA was determined to prevent and clean up etch damage caused by the atomic H. Consistent with the reduction of H induced etch damage, incorporating TMA reduced the magnitude of interface trap states at both 300 ˚C and 120 ˚C by minimizing and preventing the formation of In/Ga clusters. Lowering the temperature alone resulted in reduction of trap states, but not to the same extent as when including TMA. An *ex situ* BOE was examined on both the InGaAs (001) and (110) surfaces. The BOE efficiently removed both carbon and oxygen on the (001) surface but only removed carbon on the (110) surface. This emphasizes the need for an all dry pre-ALD surface clean when depositing material on 3D structures since this will allow for efficient nucleation of ALD precursors on all crystal planes.

4.6 Acknowledgments

Chapter 4 is in part or full, reprinted with permission from Tyler Kent, Kechao Tang, Varisthna Chobpattana, Muhammad Adie Negara, Mary Edmonds, Bhagawan Sahu, Rohit Galatage, William Mitchell, Ravi Droopad, Paul McIntyre, and Andrew C. Kummel, "The Influence of wet and dry native oxide removal on the nucleation of low temperature HfO_2 ALD on InGaAs (001) and (110) surfaces". Manuscript in preparation. The dissertation/thesis author was the primary investigator and author of this paper.

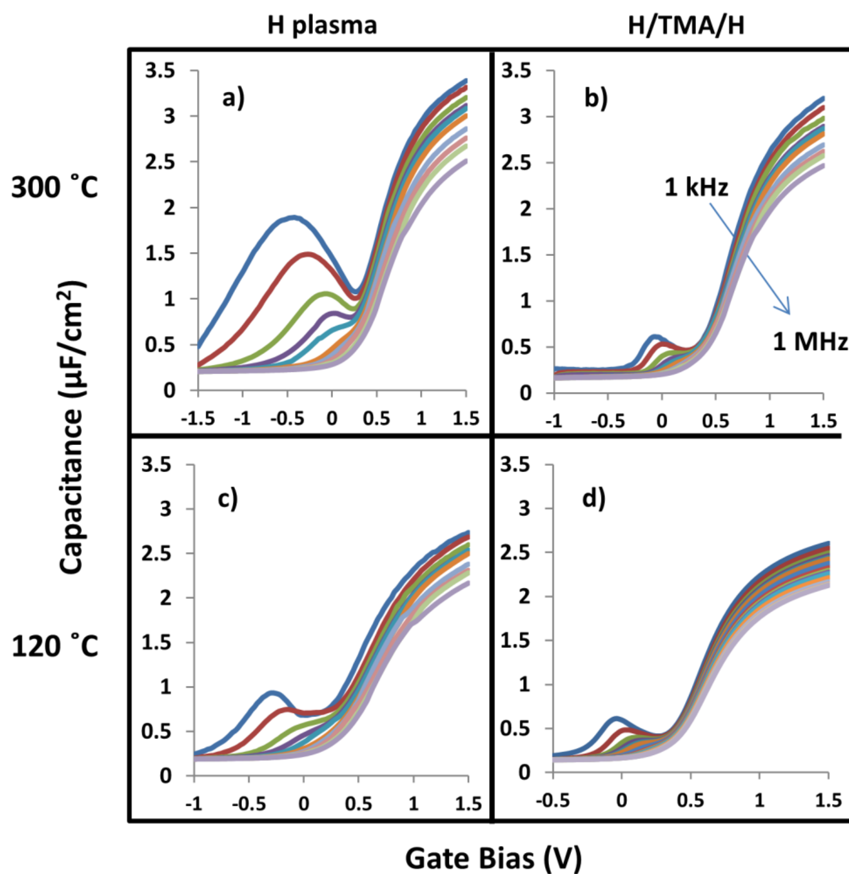

Figure 4.1. a) CV curve obtained after exposing InGaAs (001) to 10 cycles of H plasma at 300 ˚C prior to ALD. A large false inversion bump is observed which is attributed to the plasma damaging the InGaAs surface. (b) InGaAs sample exposed to 10 cycles of H/TMA/H prior to ALD at 300 ˚C. Addition of a TMA pulse dramatically reduces the magnitude of the false inversion bump suggesting it is preventing or repairing plasma damage. (c) InGaAs samples exposed to 10 cycles of H plasma only prior to ALD at 120 ˚C. False inversion bump is about reduced by 2x compared to 300 ˚C exposure confirming low temperature processing reduces plasma damage. (d) InGaAs sample exposed to 10 cycles of H/TMA/H prior to ALD at 120 ˚C. Again including TMA reduced the false inversion bump and suggests it is crucial to reducing the density of interfacial trap states.

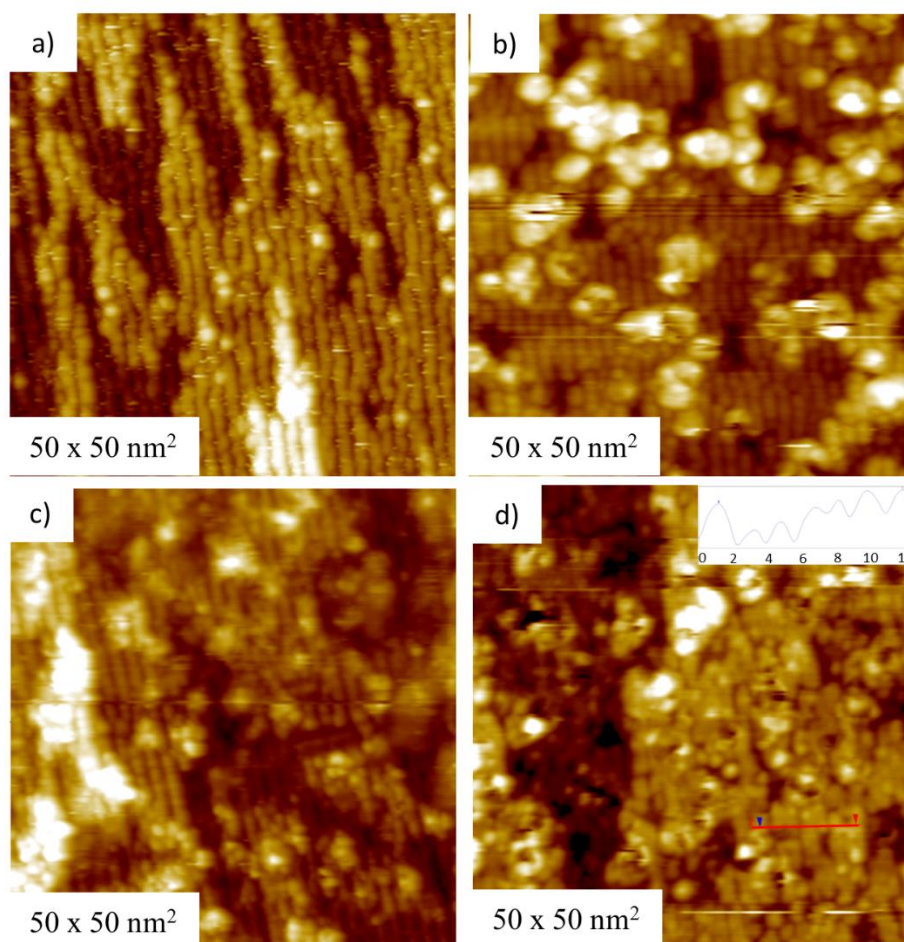

Figure 4.2. STM images of (a) clean InGaAs (2x4) surface. (b) (2x4) surface after exposure to atomic H at 300 ˚C. Formation of bright white clusters are observed with an avg. width of 5.79 nm and avg. height of 0.4 nm. (c) (2x4) surface initially exposed to TMA and subsequently atomic H, both at 300 ˚C. Density, height, and width of bright sites have been reduced. TMA may be providing alternate reaction pathways for the atomic H, such as formation and desorption of methane. (d) (2x4) surface exposed first to TMA, then atomic H, and a final dose of TMA. The white clusters are almost completely absent and the surface maintains atomic ordering (inset) and is atomically flat. This suggests TMA both prevents plasma damage as well as cleans up the remaining damage observed in (c). The TMA may react with the clusters and form volatile by products.

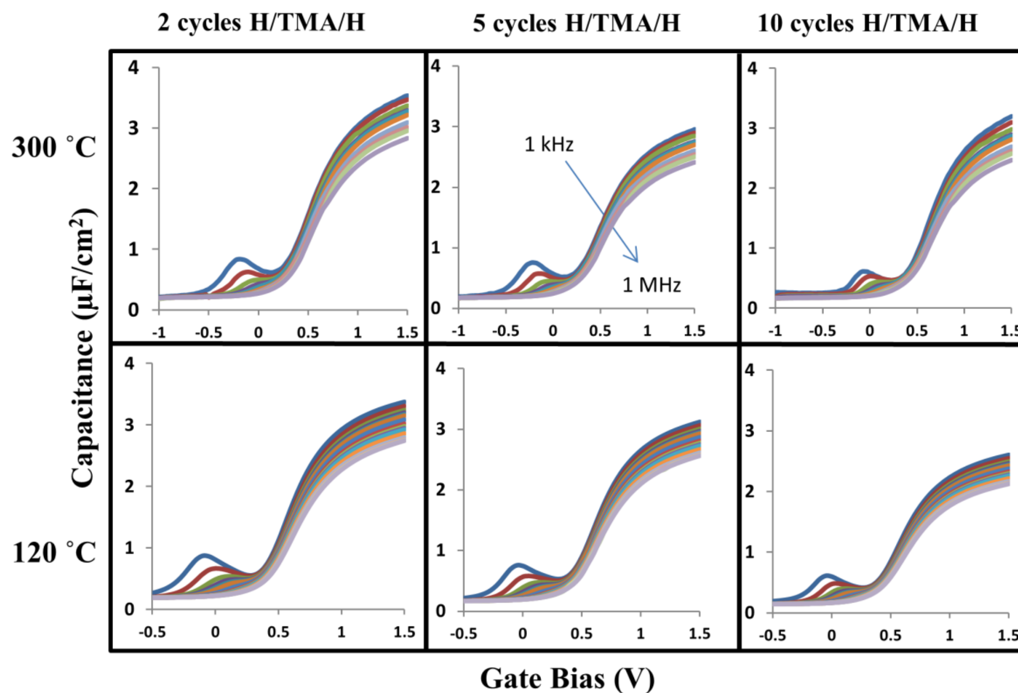

Figure. 4.3. (top row) CV curves obtained after the number of pre-ALD H/TMA/H cycles was varied at 300 ˚C. Exposing the sample to 5 or more cycles of the pre clean results in a C_{max} of ~2.4 μF/cm^2. This reduction in C_{max} compared to the 2 cycle case is attributed to an increase in nucleation density of HfO_2 which results from more efficient removal of native oxide or surface contaminants with 5 or more cycles. At 120 ˚C (bottom row) the C_{max} continually decreases as the number of cleaning cycles increases. This suggests the H plasma is not as effective at removing native oxide at lower temperatures, hence more cleaning cycles are required to maximize the nucleation density of HfO_2. It is important to note that despite a 5x increase in plasma exposure at both temperatures, the false inversion bump actually decrease indicating efficient surface cleaning by the H plasma and also the importance of TMA in protecting the surface from plasma damage.

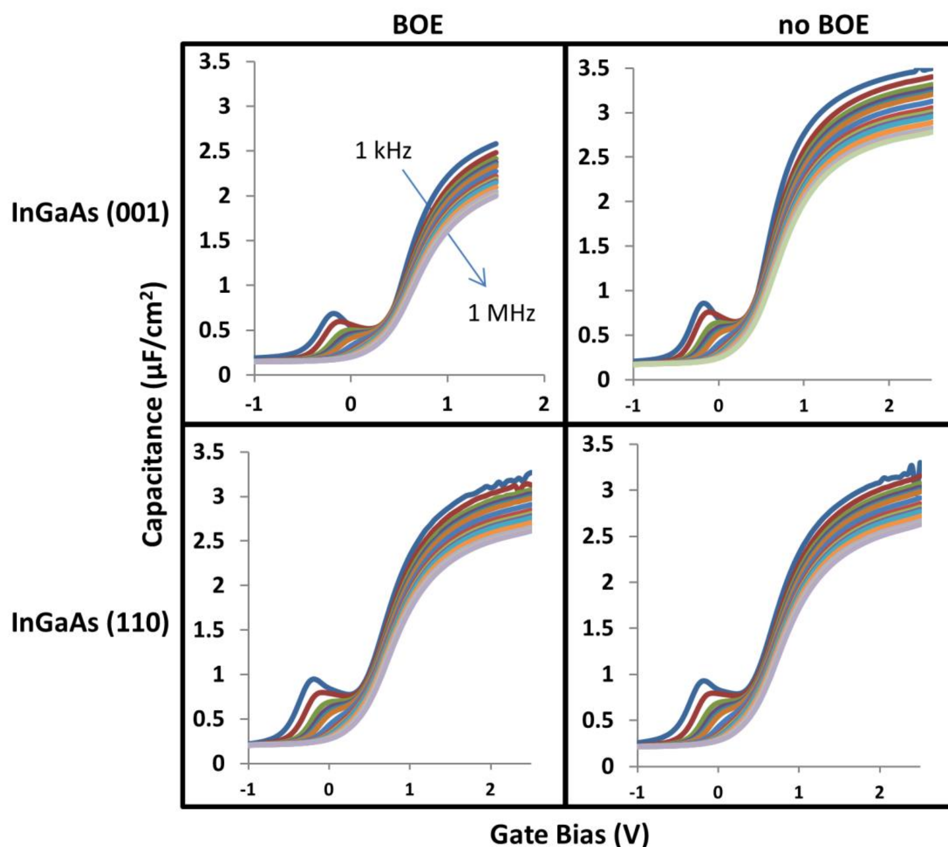

Figure 4.4. InGaAs (001) samples which did (top left) and did not (top right) receive a BOE immediately prior to ALD. (001) sample which did not receive a BOE shows a C_{max} of about 2.6 µF/cm^2 compared to 2 µF/cm^2 for the no BOE sample. It is hypothesized that the HfO_2 nucleates more efficiently on the sample which was exposed to the BOE. All 4 samples were in the ALD reactor simultaneously to ensure identical deposition conditions. (110) samples that did (bottom left) and did not receive (bottom right) a BOE prior to ALD show nearly identical CV spectra. This suggests the BOE is not effective on the (110) surface and emphasizes the need for an *in situ* dry etch which can clean both surfaces effectively.

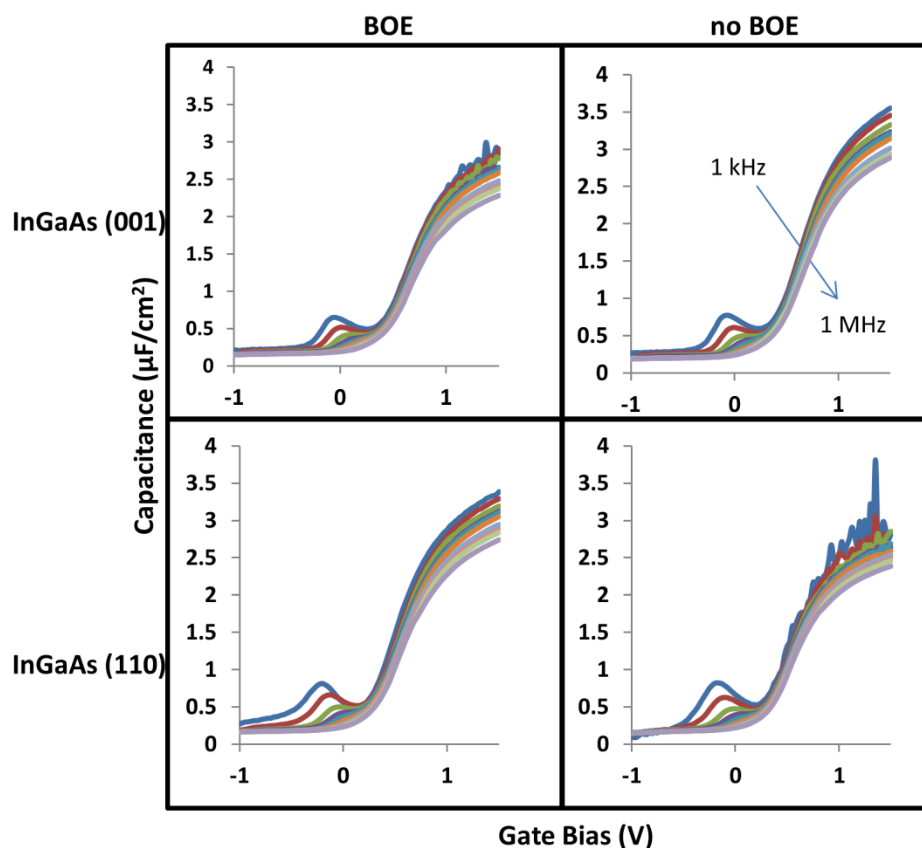

Figure 4.5. CV curves of InGaAs (001) samples which did (top left) and did not (top right) receive a BOE immediately prior to ALD at 300 ˚C. (001) sample which did not receive a BOE shows a C_{max} of about 2.8 μF/cm^2 compared to 2.4 μF/cm^2 for the no BOE sample. It is hypothesized that the HfO_2 nucleates more efficiently on the sample which was exposed to the BOE. All 4 samples were in the ALD reactor simultaneously to ensure identical deposition conditions. For the (110) samples, the C_{max} of the sample which did not receive a BOE is within 10% of the C_{max} of the BOE sample and thus not material.

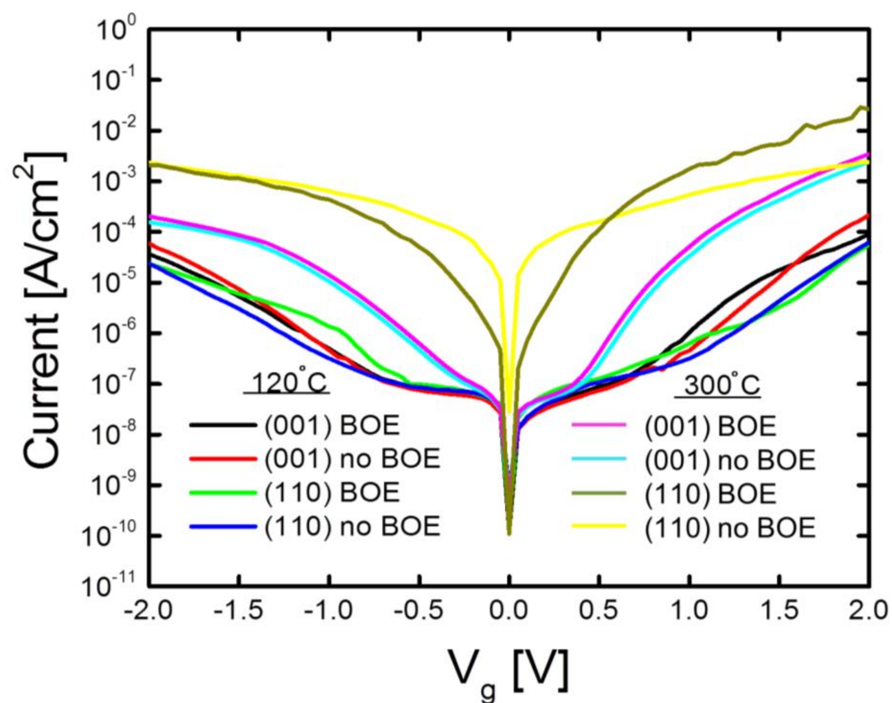

Figure 4.6. Leakage current densities of the wet and non-wet cleaned (001) and (110) samples at 120 ˚C and 300 ˚C. The 120 ˚C samples exhibit significantly lower leakage currents than the 300 ˚C samples at biases above the V_{fb} and when less than -1 V, relative to the $V_{fb.}$ It is hypothesized this is a result of the small CVD component (~1.4 Å/cycle) that was observed in the 120 ˚C ALD which would fill any pin holes that were not present in the 300 ˚C ALD which had a typical growth rate of ~1Å/cycle.

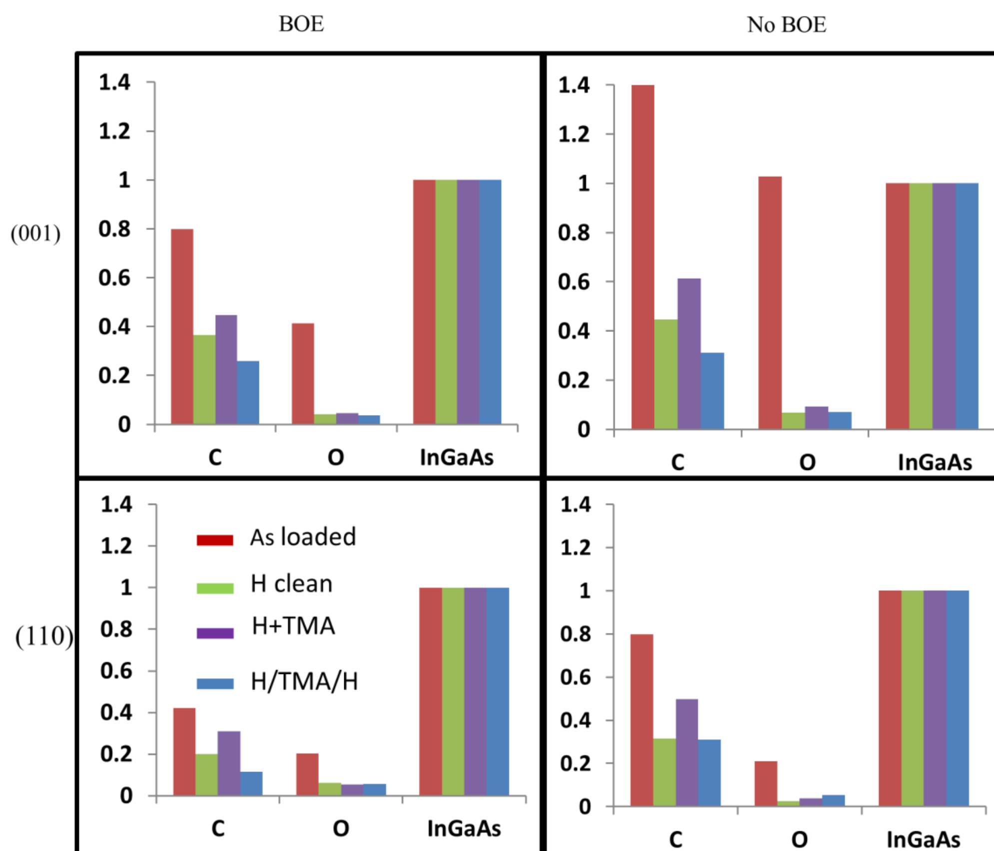

Figure 4.7. XPS data before, during, and after H/TMA/H pre-ALD surface clean. The carbon and oxygen signals are normalized to the sum of the substrate peaks. For the (001) samples (top row) the amount of C and O is reduced when receiving a BOE for the as-loaded samples (red). The (110) sample (bottom row) shows a reduction in C but no change in the amount of O for the as-loaded samples (red). This suggests the (110) surface is less prone to oxidation and explains the similar CV curves observed in Fig. 4. After exposing the surfaces to atomic H (green) the amount of C and O are reduced to similar level for the (001) and (110) samples. This demonstrates the effectiveness of a dry etch compared the wet clean on both surfaces. A dose of TMA (purple) results in a small increase in C signal due to the presence of methyl groups. A final dose of atomic H reduces the C signal from methane desorption.

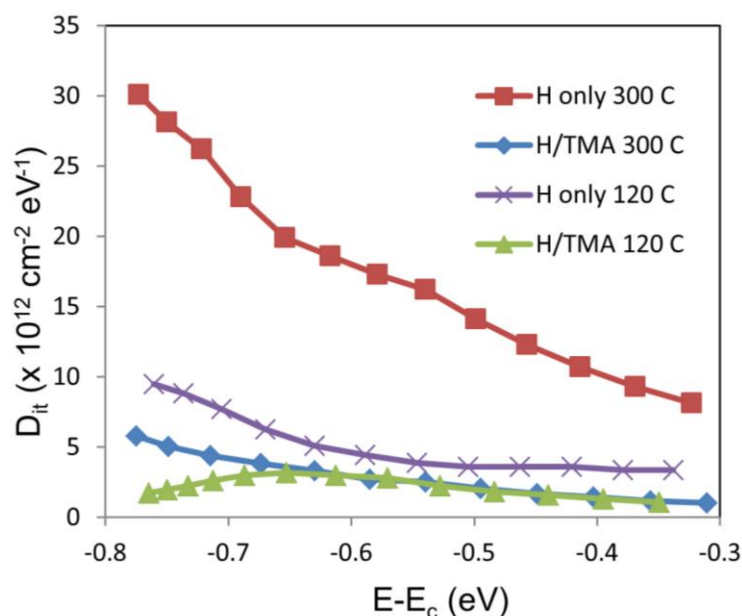

Figure 4.8. D_{it} extracted using the full interface state model. The sample which was exposed to H plasma only at 300 ˚C (red square) exhibits a much higher D_{it} than any of the other samples which is a result of plasma induced damage. The sample exposed to H plasma at 120 ˚C (purple x) shows a slightly higher D_{it} in the upper half of the bandgap compared to the other samples. This again is attributed to plasma damage. The samples exposed to H/TMA/H at 120 ˚C and 300 ˚C (green triangles, blue diamond)) exhibit the lowest D_{it} of the samples modeled and is slightly lower than at 300 ˚C. All samples which had TMA incorporated into the pre-ALD surface clean exhibit very similar D_{it} values in the upper half of the bandgap regardless of temperature or *ex situ* wet cleans. This emphasizes the importance of TMA in the *in situ* clean to allow for pristine surfaces regardless of crystal face.

Table 4.1. Peak D_{it} and N_{bt} densities. Samples which received H/TMA/H treatment have N_{bt} densities between 1.9 and 2.2 x 10^{20} $cm^{-3}eV^{-1}$. The sample which received exposure to H plasma only at 300 ˚C exhibits a much higher density of border traps. This indicates TMA reduces the number of trap states at the InGaAs/HfO_2 interface and minimizes defects in the oxide. All samples which had TMA incorporated into the pre-ALD clean have D_{it} values between 2.0 and 3.8 x 10^{12} cm^{-2} eV^{-1} whereas the samples exposed to H alone at 120 ˚C has 3.8 x 10^{12} cm^{-2} eV^{-1} and the sample exposed to H alone at 300 ˚C has 14 x 10^{12} cm^{-2} eV^{-1}. Thus TMA plays an important role in minimizing both interface defects and border traps regardless of crystal face, temperature, or *ex situ* wet cleans. It is noted that the 120 ˚C sample consistently had a lower D_{it} than the 300 ˚C sample; a statistical analysis was performed which showed this difference had a p value of < 0.05.

	V_{fb} (V)	C_{ox} (uF/cm^2)	N_{bt} ($\times 10^{20} cm^{-3} eV^{-1}$) @ $E-E_c$ = 0.5 V	D_{it} (x 10^{12} $cm^{-2}eV^{-1}$) @ $E-E_c$ = 0.5 V
(001) 10 cycles H only (120/ 300 ˚C)	0.63/0.53	4.3/5.3	2.2/3.0	3.8/14
(001) 2 cycles H/TMA (120 /300 ˚C)	0.57/0.50	4.8/6.5	1.8/2.0	3.8/3.5
(001) 5 cycles H/TMA (120 /300 ˚C)	0.55/0.50	4.5/4.9	1.7/1.9	2.7/3.3
(001) 10 cycles H/TMA (120 /300 ˚C)	0.60/0.62	3.7/5.5	1.9/2.2	2.0/2.0
(001) BOE (120 / 300 ˚C)	0.57/0.63	3.8/4.8	2.3/2.1	2.9/3.4
(001) No BOE (120 / 300 ˚C)	0.56/0.60	5.2/6.8	2.4/2.0	2.8/3.4
(110) BOE (120 / 300 ˚C)	0.59/0.50	4.5/6.0	2.2/1.9	2.8/3.2
(110) No BOE (120 / 300 ˚C)	0.59/0.55	4.6/5.5	2.1/2.0	2.8/3.5

4.7 References

[1] F. Hamzaoglu and M. R. Stan, in *Proceedings of the 2002 international symposium on Low power electronics and design* (ACM, 2002), p. 60.

[2] T. N. Theis and P. M. Solomon, Proceedings of the IEEE **98**, 2005 (2010).

[3] J. Maserjian, Journal of Vacuum Science and Technology **11**, 996 (1974).

[4] S. Lo, D. Buchanan, Y. Taur, and W. Wang, Electron Device Letters, IEEE **18**, 209 (1997).

[5] L. Kang, B. H. Lee, W.-J. Qi, Y. Jeon, R. Nieh, S. Gopalan, K. Onishi, and J. C. Lee, Electron Device Letters, IEEE **21**, 181 (2000).

[6] D.-H. Kim, et al., in *Electron Devices Meeting (IEDM), 2014 IEEE International* (IEEE, 2014), p. 25.2. 1.

[7] L. Chu, C. Merckling, A. Alian, J. Dekoster, J. Kwo, M. Hong, M. Caymax, and M. Heyns, Applied Physics Letters **99**, 042908 (2011).

[8] P. D. Ye, Journal of Vacuum Science & Technology A: Vacuum, Surfaces, and Films **26**, 697 (2008).

[9] W. Mönch, *Semiconductor surfaces and interfaces* (Springer, 2001).

[10] J. Robertson, Applied Physics Letters **94**, 152104 (2009).

[11] W. Melitz, J. Shen, T. Kent, A. C. Kummel, and R. Droopad, Journal of Applied Physics **110**, 013713 (2011).

[12] A. D. Carter, W. J. Mitchell, B. J. Thibeault, J. J. Law, and M. J. Rodwell, Applied physics express **4**, 091102 (2011).

[13] V. Chobpattana, J. Son, J. J. M. Law, R. Engel-Herbert, C.-Y. Huang, and S. Stemmer, Applied Physics Letters **102** (2013).

[14] C. Driemeier, E. Gusev, and I. Baumvol, Applied Physics Letters **88**, 201901 (2006).

[15] H.-P. Chen, Y. Yuan, B. Yu, J. Ahn, P. C. McIntyre, P. Asheck, M. J. Rodwell, and Y. Taur, IEEE Transactions on Electron Devices **59**, 2383 (2012).

[16] J. Shen, D. L. Winn, W. Melitz, J. B. Clemens, and A. C. Kummel, ECS Transactions **16**, 463 (2008).

[17] W. Melitz, T. Kent, A. C. Kummel, R. Droopad, M. Holland, and I. Thayne, The Journal of Chemical Physics **136**, 154706 (2012).

[18] H.-C. Lin, W.-E. Wang, G. Brammertz, M. Meuris, and M. Heyns, Microelectronic Engineering **86**, 1554 (2009).

[19] R. Engel-Herbert, Y. Hwang, and S. Stemmer, Journal of Applied Physics **108**, 124101 (2010).

[20] C. Hinkle, et al., Applied Physics Letters **92**, 071901 (2008).

[21] F. S. Aguirre-Tostado, M. Milojevic, C. L. Hinkle, E. M. Vogel, R. M. Wallace, S. McDonnell, and G. J. Hughes, Applied Physics Letters **92** (2008).

[22] O. M'hamedi, F. Proix, and C. Sebenne, Semiconductor science and technology **2**, 418 (1987).

[23] J. Schaefer, T. Allinger, C. Stuhlmann, U. Beckers, and H. Ibach, Surface science **251**, 1000 (1991).

[24] J. Tersoff, Physical Review Letters **52**, 465 (1984).

[25] T. Nishimura, K. Kita, and A. Toriumi, Applied Physics Letters **91**, 123123 (2007).

[26] W. Melitz, E. Chagarov, T. Kent, R. Droopad, J. Ahn, R. Long, P. C. McIntyre, and A. C. Kummel, in *Electron Devices Meeting (IEDM), 2012 IEEE International*, 2012), p. 32.4.1.

[27] H.-P. Chen, J. Ahn, P. C. McIntyre, and Y. Taur, Journal of Vacuum Science & Technology B **32**, 03D111 (2014).

[28] C. W. Wilmsen, (1985).

[29] B. Brennan and G. Hughes, Journal of Applied Physics **108**, 053516 (2010).

[30] J. J. Barton, W. A. Goddard, and T. McGill, Journal of Vacuum Science and Technology **16**, 1178 (1979).

[31] J. L. A. Alves, J. Hebenstreit, and M. Scheffler, Physical Review B **44**, 6188 (1991).

[32] Y. Yuan, B. Yu, J. Ahn, P. C. McIntyre, P. M. Asbeck, M. J. Rodwell, and Y. Taur, Electron Devices, IEEE Transactions on **59**, 2100 (2012).

[33] D. Fleetwood, M. Shaneyfelt, W. Warren, J. Schwank, T. Meisenheimer, and P. Winokur, Microelectronics Reliability **35**, 403 (1995).